

AFFINITY CHROMATOGRAPHY USING CONCATEMERIC DNA

M.Sc. Thesis – E.Q. Kapteyn – McMaster University – Chemical Biology

AFFINITY CHROMATOGRAPHY USING CONCATEMERIC FUNCTIONAL
NUCLEIC ACIDS FOR BIOSENSING

By EMILY QUINN KAPTEYN, B.Sc. (Honours)

A Thesis Submitted to the School of Graduate Studies in Partial Fulfilment of the
Requirements for the Degree Master of Science

McMaster University © Copyright by Emily Kapteyn, March 2018

M.Sc. Thesis – E.Q. Kapteyn – McMaster University – Chemical Biology

MASTER OF SCIENCE (2017) McMaster University

(Chemical Biology) Hamilton, ON

TITLE: Affinity Chromatography Using Concatemeric Functional
 Nucleic Acids for Biosensing

AUTHOR: Emily Q. Kapteyn, B.Sc. (Honours) (McMaster University)

SUPERVISOR: John D. Brennan

NUMBER OF PAGES: xiv, 87

ABSTRACT

This thesis describes the use of functional nucleic acid (FNA) superstructures entrapped within monolithic macroporous sol-gel-derived silica for solid-phase flow-based sensing of small molecules and macromolecular proteins. The work described herein overcomes a long-standing issue with entrapment of biomolecule into sol-gel-derived materials; the mesoporous pore morphology required to retain entrapped biomolecules prevents detection of large analytes as these can't access the entrapped species. It is shown that large DNA superstructures can be produced through rolling circle amplification of a functional nucleic acid, resulting in concatemeric FNA species with diameters of several microns. Such species can be entrapped within macroporous sol-gel derived materials with micron-sized pores with minimal leaching, thus allowing for detection of a wide range of molecules, including biomolecules. Optimal materials for entrapment of FNA superstructures was achieved using a high-throughput material screening method, which minimized biomolecule leaching while maintaining FNA activity. Using an optimized material, concatemeric aptamer superstructures were entrapped within macroporous monolithic columns for flow-based detection of small molecules and proteins, extending the range of analytes that can be analyzed using biohybrid monolithic columns. Preliminary studies on the formation and properties of a DNAzyme superstructure for detection of *E. coli* detection were also performed, which provided valuable information on factors that must be controlled to allow reproducible fluorescence-based detection of *E. coli* using the crude intracellular matrix as the target.

ACKNOWLEDGEMENTS

I would like to thank John D. Brennan for giving me the opportunity to complete my graduate school work in his lab. Dr. Brennan, along with the other member of my supervisory committee, Dr. Fred Capretta, provided much needed guidance and advice when completing my projects. I would also like to thank the past and present members of the Brennan group, and the technicians at the Biointerfaces Institute for their advice and support. In particular, I would like to thank Dawn White for her patience when listening to my complaints and difficulties with my project. I would also like to acknowledge my family and friends for supporting me throughout the completion of my program. Specifically, I want to thank my parents for giving me a place to live with free food and supporting me whole-heartedly through the duration of my program.

TABLE OF CONTENTS

Abstract.....	iii
Acknowledgements.....	iv
Table of Contents.....	v
List of Figures.....	vii
List of Tables.....	xii
List of Abbreviations.....	xiii
Declaration of Academic Achievement.....	xv
CHAPTER 1 INTRODUCTION.....	1
1.1 Thesis Overview.....	1
1.2 Literature Review.....	3
1.2.1 Sol–Gel Process.....	3
1.2.2 Sol–Gel-Derived Monolithic Columns.....	6
1.2.3 Functional Nucleic Acids.....	9
1.2.4 Rolling Circle Amplification and Concatenated DNA Species.....	14
1.3 Thesis Goals.....	16
1.4 References.....	18
CHAPTER 2 SOL-GEL DERIVED BIOHYBRID MATERIALS INCORPORATING LONG-CHAIN DNA APTAMERS.....	25
Author’s Preface.....	25
2.1 Abstract.....	26
2.2 Introduction.....	27
2.3 Results and Discussion.....	28
2.4 Conclusions.....	37
2.5 Experimental.....	37
2.5.1 Materials.....	37
2.5.2 Methods.....	38
2.6 Acknowledgements.....	45
2.7 References.....	46
2.8 Appendix.....	49

CHAPTER 3 | EVALUATION OF DNAZYME-BASED NANOFLOWERS FOR BACTERIAL DETECTION.....62

Author’s Preface.....	62
3.1 Abstract.....	63
3.2 Introduction.....	64
3.3 Experimental.....	66
3.3.1 Materials.....	66
3.3.2 Methods.....	67
3.4 Results and Discussion.....	71
3.5 Conclusions.....	78
3.6 References.....	79
3.7 Appendix.....	81

CHAPTER 4 | CONCLUSIONS.....85

4.1 Summary and Future Outlook.....	85
4.2 References.....	87

LIST OF FIGURES

Figure 1.1. Compositions for the fabrication of biomolecule compatible sol–gel-derived materials. (Adapted from Brennan <i>et al.</i> 2007, Ref #24).....	5
Figure 1.2. SEM images of a protein-doped monolithic column (A), and the bimodal pore distribution commonly present in these monolithic columns (B). (Adapted with permission from Hodgson <i>et al.</i> , Ref #3 © 2004 American Chemical Society.).....	8
Figure 1.3. Schematic of a structure-switching aptamer in the tripartite (left) and bipartite (right) conformations. The tripartite complex is composed of three DNA strands hybridized together prior to target addition. The structure of the aptamer changes shape upon target addition and the dabcyl quencher strand (cQDNA) is released. The bipartite complex is similar to the tripartite strand, however the fluorophore is covalently linked to the aptamer strand instead. (Adapted from Carrasquilla <i>et al.</i> 2013, Ref #39).....	11
Figure 1.4. Schematic representation of the method for target binding to the DNAzyme EC1 in the <i>cis</i> -conformation. (Reproduced from Zhang <i>et al.</i> 2016, Ref # 73).....	13
Figure 1.5. Schematic of rolling circle amplification to produce concatemeric DNA using a circular template, primer and phi29 DNA polymerase. The primer extends in the 5'→3' direction.....	15
Figure 1.6. SEM image showing a typical DNA nanoflower that self-assembled after performing RCA for 10 hours. (Adapted with permission from Zhu <i>et al.</i> , Ref #15 © 2013 American Chemical Society).....	16
Figure 2.1. Opacity pots of sol-gel derived materials. Percent transmittance of a) SS, b) TMOS, c) 40% TMMS (in TMOS), and d) MTMS sols mixed in assay buffer with 0 – 10 kDa PEG at various concentrations after 3 h gelation at room temperature. Materials with transmittance ≤ 20% are considered to be macroporous.....	29
Figure 2.2. Aptamer leaching from sol-gel derived materials. The percent leaching of a) ATP concatemers versus monomers and b) PDGF concatemers versus monomers entrapped in various mesoporous or macroporous sol-gel derived materials. C) schematic of concatemers entrapped within a macroporous matrix.....	31

Figure 2.3. Signal response comparison of aptamer reporters. Fluorescence from a) ATP-binding monomer and concatemer with 2 mM ATP or b) PDGF-binding monomer and concatemer with 200 nM PDGF in various mesoporous or macroporous materials. The red line in a) and b) indicates a normalized F/F_0 of 1.0 (no signal increase). Response of c) ATP-binding concatemer with 0 – 3 mM ATP or d) PDGF-binding concatemer with 0 – 300 nM PDGF in Meso or Macro 40% MTMS.....33

Figure 2.4. SEM images of sol-gel derived monolithic columns. Magnified images of a monolithic column with or without entrapped concatemeric aptamers formed in a 250 μm i.d. capillary using SEM analysis of non-conductive materials.....35

Figure 2.5. Target detection using aptameric monolithic columns. A) Schematic of macroporous sol-gel derived monolith containing concatemeric aptamers and target binding-induced release of F'DNA. B) ATP concatemer column response to 0 – 300 nM PDGF. Insets: representative fluorescence scans of eluate fractions upon target addition – b) 2 mM ATP or c) 200 nM PDGF.....36

Figure S2.1. Time-resolved changes in transmittance of sol-gel derived materials. Transmittance at 400 nm of SS (top) and 40% MTMS (bottom) mixed in assay buffer with 0 – 10 kDa PEG at various concentrations over 12 h as samples undergo phase separation and evolve over time.....49

Figure S2.2. DLS measurements of DNA constructs in solution. Hydrodynamic size distributions of a) concatemeric, b) monomeric and c) circular template constructs for the ATP aptamer (top) and PDGF aptamer (bottom) in solution as measured by dynamic light scattering intensity.....50

Figure S2.3. Signal enhancement of concatemeric reporters in PEG-doped buffer. Fluorescence signal response of the a) concatemeric ATP aptamer with 2 mM ATP and b) concatemeric PDGF aptamer with 200 nM PDGF, in solution containing increasing concentrations of 1.25 – 10 kDa PEG.....51

Figure S2.4. Selectivity of entrapped concatemeric aptamers. Selectivity of the a) concatemeric ATP aptamer to different nucleotides at 2 mM concentration and b) concatemeric PDGF aptamer to different growth factors and proteins at 200 nM concentration, entrapped in Macro 40% MTMS.....52

Figure S2.5. Concatemeric aptamer emission intensity upon exposure to DNase I. Fluorescence measurements over time (1 hr) after addition of 1 unit of DNase I to the ATP-binding and PDGF-binding concatemeric aptamer reporters in solution or entrapped within the Macro 40% MTMS material.....53

Figure S2.6. Backpressure of monolithic columns upon aging. Backpressure of monolithic columns relative to empty capillaries (indicated by a relative backpressure of 1 at ~15 PSI) after various aging periods at a flow rate of 1 $\mu\text{L}/\text{min}$. Columns were used for target detection assays only after at least 7 days of aging.....	54
Figure S2.7. EDX analysis of sol-gel derived monolithic columns. A spectral overlay comparing the differences in elemental composition between a monolithic column with versus without entrapped concatemeric aptamers. Inset: the relative atomic contribution from C, N, O and Si for a sol-gel derived monolithic column with or without entrapped concatemeric aptamer amplicons.....	55
Figure S2.8. Fluorescence Scans of Column Fractions. Emission scans of eluate from monolithic columns containing various entrapped DNA molecules, divided into four fractions: a) pre-wash 1, b) pre-wash 2, c) elution with target and d) post-target wash. Fractions 1, 2 and 4 serve as wash steps with buffer only and fractions 3 contains either 2 mM ATP (top) or 200 nM PDGF (bottom) for the appropriate column.....	56
Figure S2.9. Column response to PDGF in a complex sample. PDGF concatemer-doped monolithic column response to 0 or 200 nM PDGF in either buffer or undiluted human serum.....	57
Figure S2.10. Response of mixed concatemer columns. Columns containing both PDGF-FAM and ATP-Cy5 concatemers were exposed to either 2 mM ATP (red line), 200 nM PDGF (green line) or a mixture of 200 nM PDGF and 2 mM ATP in buffer (blue line). Left spectra show emission of FAM originating from the PDGF aptamer, right spectra show emission of Cy5 originating from the ATP aptamer.....	58
Figure 3.1. TEM images of the DNA nanoflowers.....	72
Figure 3.2. SEM images of the DNA nanoflowers in (A,B) solution and (C,D) after incubation in <i>E. coli</i> CIM for 1 hour. The solutions were solvent evaporated on nitrocellulose paper.....	73
Figure 3.3. Optimization of the FS28 cleavage reaction using (A) 1.0 μM , (B) 1.5 μM , and (C) 2.0 μM of the various DNAzyme constructs. The background fluorescence produced in wells containing EC1M was subtracted from each construct over time. Initial fluorescence (F_0) corresponded to the fluorescence intensity immediately after adding 25 % (v/v) of the CIM (without heating). The nanoflower construct consistently exhibited greater fluorescence enhancement (F/F_0) than the monomer and 2D DNAzyme constructs.....	75

Figure 3.4. The fluorescence enhancement produced by the cleavage of FS28 (50 nM) by the three different DNAzyme types (1 μ M) in the presence of *E. coli* CIM or *B. subtilis* CIM. The background fluorescence produced by EC1M was subtracted from each measured value. The initial fluorescence corresponded to the fluorescence intensity measured immediately after adding the CIM to the wells.....77

Figure S3.1. Circle ligation was successful (lanes 2 and 3), as indicated in the 10 % dPAGE gel used for purification. Despite the circle having the same molecular weight as the linear circle (lane 1, band above smeared dye), the circle cannot move through the gel as easily which results in a shifted band. The primer is present near the bottom of the gel.....81

Figure S3.2. RCA of the purified circle resulted in thick bands with smearing on the 0.6 % agarose gel, which indicates concatemers present in the sample (lanes 1 and 2). Lane 3 shows the results of the negative control, meanwhile lane 4 contains only circle.....82

Figure S3.3. Restriction enzyme digestion produced DNA strands of various lengths based on the extent of digestion that occurred on the various sized concatemers. The negative control did not contain restriction enzyme, which accounts for the thick smear. The bottom band corresponds to the size of the monomer.....83

LIST OF TABLES

Table S2.1. DNA oligonucleotide sequences for aptamer reporter systems.....	59
Table S2.2. Composition of the 24 macroporous sol-gel derived materials chosen for aptamer entrapment.....	60
Table S2.3. Fluorescence polarization from ATP or PDGF concatemer, monomer and FDNA in solution or leached from materials.....	61
Table S3.1. Sequences of the DNA oligonucleotides used in this work.....	84

LIST OF ABBREVIATIONS

ALP	alkaline phosphatase
ATP	adenosine 5'-triphosphate
BSA	bovine serum albumin
CIM	crude intracellular matrix
CTP	cytidine 5'-triphosphate
DABCYL	4-(dimethylaminoazo)benzene-4-carboxylic acid
DGS	diglycerylsilane
DLS	dynamic light scattering
DNA	deoxyribonucleic acid
DNase	deoxyribonuclease
dNTPs	2'-deoxyribonucleoside 5'-triphosphates
dPAGE	denaturing polyacrylamide gel electrophoresis
EDX	energy dispersive x-ray spectroscopy
EGF	epidermal growth factor
FDNA	fluorophore-labeled DNA
FNAs	functional nucleic acids
FRET	fluorescence resonance energy transfer
FS28	ribonucleotide containing fluorogenic substrate
FQU28	exclusively deoxyribonucleotide fluorogenic substrate
GTP	guanosine 5'-triphosphate
HPLC	high-performance liquid chromatography

IGF-I	insulin-like growth factor
γ -MAPS	γ -methacryloxypropyltrimethoxysilane
MREs	molecular recognition elements
MSQ	methylsilsequioxane
MTMS	methyltrimethoxysilane
MW	molecular weight
PDGF	platelet-derived growth factor
PEG	polyethylene glycol
QDNA	quencher-labeled DNA
RCA	rolling circle amplification
RNA	ribonucleic acid
SELEX	systematic evolution of ligands by exponential enrichment
SEM	scanning electron microscopy
SS	sodium silicate
T4 PNK	T4 polynucleotide kinase
TEM	transmission electron microscopy
TEOS	tetraethylorthosilicate
TMOS	tetramethylorthosilicate
UTP	uridine 5'-triphosphate

DECLARATION OF ACADEMIC ACHIEVEMENT

This thesis describes the research performed for the development of sol–gel-derived silica capillary columns with two different types of functional nucleic acids entrapped within the macropores. The entrapment of functional nucleic acids along capillary columns has not been previously reported in the literature.

Chapter 2 discusses the sol–gel entrapment of structure-switching aptamers for biosensing ATP and platelet-derived growth factor along capillary columns. Carmen Carrasquilla and the author fabricated the columns and performed the biosensing assays along the capillary columns. The author performed scanning electron microscopy analysis, including elemental distribution analysis on the silica-based columns. Carmen Carrasquilla performed the data analysis from the materials screen and biosensing assays. The author, Carmen Carrasquilla, Dr. Yingfu Li, and Dr. John Brennan wrote the manuscript.

Chapter 3 contains research performed exclusively by the author for the development of macroporous sol–gel-derived silica capillary columns with entrapped concatenated DNAzyme for *Escherichia coli* detection. The author performed all data analysis and wrote the manuscript with Dr. John Brennan.

Dr. John Brennan supervised and provided advice for all of the research in this thesis. In addition, Dr. Fred Capretta provided recommendations in regards to this research.

CHAPTER 1 | INTRODUCTION

1.1 Thesis Overview

Solid-phase bioassays require biomolecule immobilization for use of miniaturized platforms that minimize reagent volumes and allow washing steps. One such biomolecule immobilization method uses sol–gel entrapment, which has been used in many different solid-phase bioassay formats,¹ including thin films, microwell plates, microarrays, and monolithic capillary-scale columns. The bio/inorganic hybrid sol–gel-derived materials are limited to investigating small molecule (generally < 2 kDa) interactions however,² due to the requirement to use mesopores with diameters less than 10 nm for biomolecule entrapment. The retention of the biomolecule within the pores is based on size exclusion and large macromolecules, such as proteins, cannot diffuse to the regions containing the biomolecule that act as the recognition element.³

Developing a method for biomolecule entrapment within macropores (diameters > 50 nm) may allow the investigation of macromolecular interactions using sol–gel-derived biohybrid materials. Macroporous materials have been limited to using covalent or affinity-based interactions to immobilize the biorecognition element to prevent leaching from the materials.^{4–9} Covalent or affinity-based immobilization can be a cumbersome process as it requires several steps after the material has aged sufficiently. In addition, the biomolecule may become denatured and generally has a lower loading capacity than sol-gel entrapment. The entrapment of biomolecules that are large enough to be retained within the micron-sized pores is an alternative method for immobilization. The range of

targets available for detection using macroporous sol–gel-derived biohybrids would expand to include proteins if the biomolecules could be retained.

The biomolecules would need to be larger for retainment within the macropores however, and proteins have an inherent size that cannot be changed, which makes most proteins unsuitable for entrapment. In contrast, rolling circle amplification (RCA) can be used to elongate functional nucleic acids (FNAs) into concatemeric aptamers or DNAzymes that are MDa in size,¹⁰ which we theorized would be large enough for biomolecule retainment within macroporous sol–gel-derived silica. Concatenated DNA species have been used as the recognition element in solid-phase bioassays, as reported by several groups, including those of Willner and Tan.^{11–14} In addition, these concatenated species can become large DNA superstructures (referred as nanoflowers) that are microns in size,¹⁵ which may further aid in biomolecule retainment.

The overall goal of this research was to investigate the potential for using concatenated DNA species, including DNA aptamers and DNAzymes, as the biorecognition element within sol–gel-derived materials, and to further the use of sol-gel entrapped biomolecules beyond the current small molecule limit by applying these bio/inorganic hybrid columns to biosensing and affinity chromatography of high molecular weight analytes. The concatemeric form of the DNA aptamers was optimized in solution in previous reports,¹⁰ however the chosen concatenated DNAzyme has not been investigated previously, so the DNAzyme needed to be optimized in solution prior to material entrapment.

1.2 Literature Review

1.2.1 Sol–Gel Process

The sol-gel process is a room temperature, biofriendly method for the fabrication of porous glass-like materials that have the ability to encapsulate biomolecules, such as proteins and DNA, in their native form.^{16,17} The sol-gel matrix can be derived from an organic,¹⁸ inorganic,¹⁹ or hybrid precursor.²⁰ The sol-gel process is an efficient method for the entrapment of biomolecules on microfluidic and microarray chips.^{21–23} It is also an excellent method to create monolithic capillary columns with high bed volumes and surface area to maximize affinity interactions with the entrapped biomolecule.²⁴ The first sol-gel entrapment of a biomolecule was accomplished by Braun *et al.* in 1990, using the enzyme alkaline phosphatase (ALP) in alkoxy-silane-derived glass.²⁵ Since then, a variety of different biological species have been immobilized within sol-gel-derived materials, including living cells, DNA, enzymes, and membrane receptors.^{16,17,26–29} Biomolecule immobilization within sol-gel-derived materials allows the efficient characterization of biomolecule interactions due to the ability to maintain the native conditions of the biomolecule.^{27,30,31}

1.2.1.1 Precursor selection

The aqueous hydrolytic processing of labile precursors to produce metal or semi-metal oxides begins the sol-gel process. Silicon oxide (SiO₂) is the most studied composition in the formation of sol-gel matrices, however the use of TiO₂,³² Al₂O₃,³³ or ZrO₂,³⁴ have been reported for biomolecule encapsulation. The hydrolysis process begins by adding water to an alkoxy precursor, such as tetramethylorthosilicate (TMOS) or

tetraethylorthosilicate (TEOS), along with a solvent that corresponds to the released by-product.¹⁶ However, precursors that release alcohol are not used for protein entrapment due to biomolecule degradation in the presence of alcohol.³⁵ Alcohol-free precursors, such as sodium silicate (SS) or diglycerylsilane (DGS), are alternative precursors for applications using proteins.^{36,37} For instance, DGS produces glycerol upon hydrolysis, which can be helpful for protein storage while maintaining protein activity. In contrast, DNA and RNA structures are not affected by alcohol, which allows TMOS and TEOS to be used as precursors for FNA entrapment.^{38,39}

1.2.1.2 Sol formation and gelation

All sol–gel-derived silica materials are formed using the same chemistry principles, regardless of the number of hydrocarbons present in the precursor (Figure 1.1).²⁴ Colloid sols form during hydrolysis, and these sols eventually begin to condense to form the porous siloxane network.²⁵ Following aging, the siloxane network forms polymerized silica in a rigid, gel-like structure. If biomolecule entrapment is desired, the biomolecules are added to the silanol solution prior to condensation. The “cage”-like network cross-links around the biomolecule to entrap it and the porous nature allows small molecules to diffuse through the pores to access the biomolecule. The large surface area enhances reactivity and the pores allow for rapid mass transfer with optimized reaction kinetics.³⁰

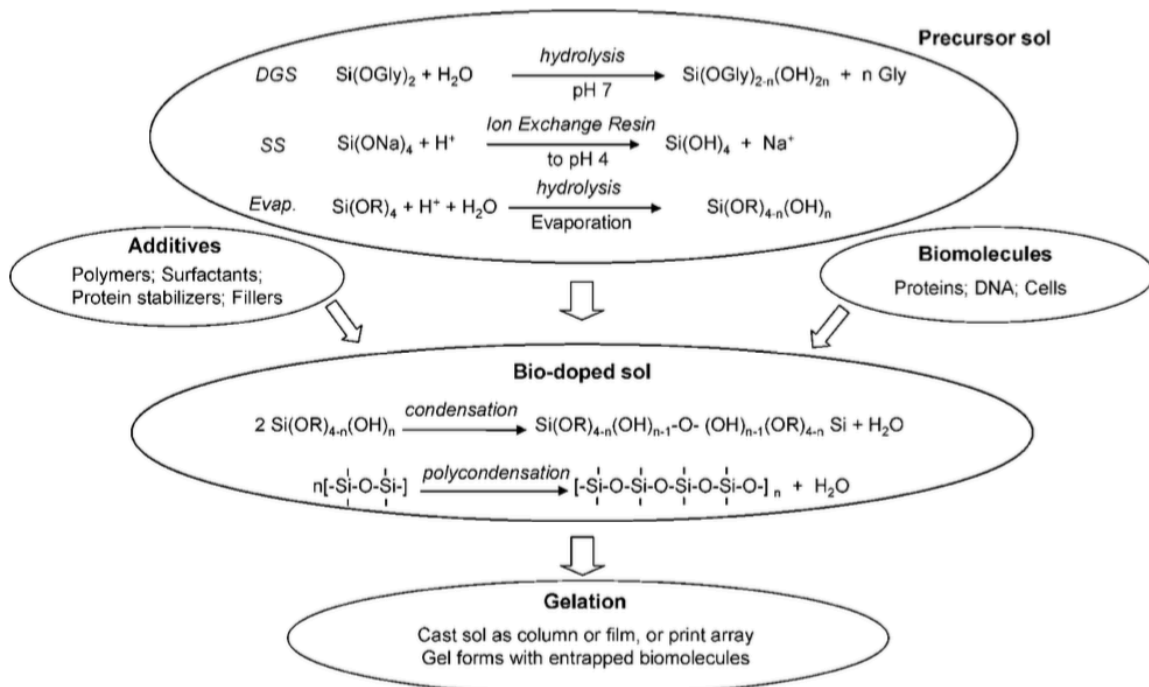


Figure 1.1. Compositions for the fabrication of biomolecule compatible sol–gel-derived materials. (Adapted from Brennan *et al.* 2007, Ref #24).

1.2.1.3 Controlling pore size

The pore size is determined by a number of factors including: precursor composition, catalyst concentration, presence of porogens, temperature, pH, phase separation time and gelation time.^{40–42} Polyethylene glycol (PEG) is commonly used as a porogen in sol–gel material formation, and the PEG concentration is inversely proportional to the rate of gel formation.³⁰ In addition, PEG reduces the shrinkage of the gel and sterically prevents pore collapse.^{19,43} The molecular weight of the PEG affects the size of the pores to control whether microporous (<2 nm in diameter), mesoporous (2 – 50 nm), or macroporous (>50 nm) matrices are formed. Pore size is dependent on the presence of PEG due to its effect on the spinodal decomposition of the sol. Spinodal decomposition is the process in which the material composition has reached a critical point such that the one-phase

thermodynamics favour the formation of two co-existing phases.⁴⁴ The co-existing phases coarsen over time to produce the final morphology of a continuous matrix with a particular pore size.

1.2.2 Sol–Gel-Derived Monolithic Columns

1.2.2.1 Monoliths

Sol–gel-derived monoliths are fabricated as homogeneous microstructures that have been shaped based on various environmental conditions, such as pH, porogen size and concentration, precursor type, and temperature.⁴⁵ The final morphology of the material can be tailored to be microporous, mesoporous, or macroporous or a hybrid of two of the pore sizes, based on the environmental conditions. Monolithic materials were developed in the early 1990s as an alternative to packing columns with functionalized particles for efficient compound separation or mixture analysis in liquid chromatography applications. Particle sizes in packed columns range from 1.5 μm to 5 μm , with the smaller particles providing more surface area for mass transfer than larger particles, but suffering from the drawback of high back pressure for constant mobile phase flow.⁴⁶ Microbore columns were used for high-efficiency separations when interfaced with high-performance liquid chromatography (HPLC) systems. These microbore columns have large bed volumes of 0.1 – 0.5 mL, which results in longer separation times and are not practical in regards to conserving reagents.^{46,47} Technological advances in liquid chromatography systems allowing accurate low flow rates at microliter or nanoliter volumes per minute resulted in the development of columns with smaller bed volumes to achieve efficient compound separation with reduced separation time.⁴⁰

The advent of monolithic materials allowed columns to become miniaturized platforms with bed volumes on the micro- or nanoscale. Monolithic column fabrication offers the additional advantage that the material can be prepared directly *in situ* by infusing the condensed sol into narrowbore columns prior to phase separation and gelation. Furthermore, monolithic pores can be carefully tuned by adjusting conditions.⁴⁴ Bimodal pore distribution can be used to optimize mass transfer kinetics while maintaining an appropriate back pressure so that flow remains consistent and accurate. The macropores allow for consistent flow while mesopores are present for the surface area required for efficient mass transfer.⁴⁰

Sol-gel-derived silica monolithic capillary columns can be used for conventional normal- or reverse-phase chromatography for the separation of small molecules within a mixture based on compound polarity.³⁰ Silica is used for normal-phase chromatography, meanwhile the silica can be functionalized with C₁₈ groups for use in reverse-phase chromatography.⁴⁶ In addition, affinity chromatography can similarly be performed by entrapping biomolecules within the monolith for compound screening or biosensing.⁴⁸⁻⁵⁰

1.2.2.2 Bio-doped monoliths

Bio-doped monolithic columns with entrapped biomolecules are fabricated by adding the protein or DNA to the condensing silica sol prior to spinodal decomposition and gelation.^{51,52} The most amenable bio-doped columns for biosensing used bimodal pore structure with macropores for efficient flow and mesopores for the surface area required for mass transfer (Figure 1.2).³ The pore morphology has to be carefully controlled however, due to significant leaching that can result when there are too many macropores

present in bimodal meso/macroporous structures.¹⁹ Initial attempts at entrapping proteins within the monolithic columns exhibited leaching of up to 70% of the entrapped protein when flow was applied to the columns.³ Tailoring the pore morphology to include more mesopores resulted in significantly more retainment of the proteins with only 20% leaching from the column during initial optimization of these protein-doped columns.¹⁹ The smaller pores are required to effectively ensure the biomolecule is not removed from the column upon initial column washes.^{3,19}

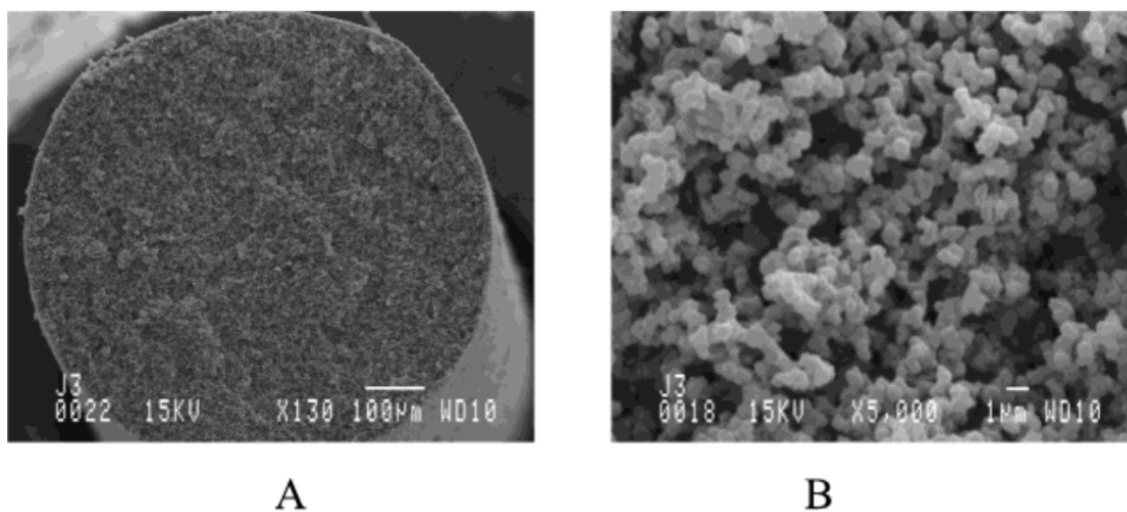


Figure 1.2. SEM images of a protein-doped monolithic column (A), and the bimodal pore distribution commonly present in these monolithic columns (B). (Adapted with permission from Hodgson *et al.*, Ref #3 © 2004 American Chemical Society.)

Size exclusion principles prevent large biomolecules, such as proteins, to enter mesopores to interact with an entrapped biomolecule, which limits mesoporous columns to detecting small molecules in biosensing and affinity chromatography assays.^{3,4,36,49,50,53–55} An exclusively macroporous column that entraps a large biomolecule is required for analyzing large macromolecules, such as proteins, in these affinity-based assays and biosensors.

Macroporous silica-based columns either require a porogen, such as PEG, to be added to the sol,¹⁹ or the precursor can be exclusively methyltrimethoxysilane (MTMS) to induce phase separation and produce macroporous methylsilsequioxane (MSQ) materials.⁴⁰ The MSQ materials have hydrophobic Si-CH₃ groups which prevent shrinkage from the capillary walls, increases pH stability, and provide high separation efficiency. All of these monolithic macroporous columns, whether exclusively composed from MTMS or a combination of other silica precursors with PEG, have not been used in biosensing applications with entrapped biomolecules however, due to extensive biomolecule leaching.^{3,19} Conventional biomolecules are too small for entrapment, so covalent or affinity-based interactions are typically used for biomolecule immobilization.^{1,4,5,8}

1.2.3 Functional Nucleic Acids

An emerging alternative to proteins as assay recognition elements is the use of functional nucleic acids (FNAs) that can be designed to selectively bind to a specific target. There are primarily two different types of FNAs that can be used as selective binding species: DNA/RNA aptamers and DNA or RNA enzymes (DNAzymes and ribozymes, respectively). Aptamers are selective binding biomolecules that can rival antibodies for their affinity for a specific target.⁵⁶ Antibodies usually have dissociation constants (K_d) ranging from 1 nM to 10 nM, whereas aptamers exhibit even greater affinities for their targets with K_d 's ranging from 1 pM to 1 nM.⁵⁷

FNAs are usually short DNA sequences containing 13 – 240 nucleotides that have been selected for using a method called systematic evolution of ligands by exponential

enrichment (SELEX) to bind to a specific target.⁵⁷ SELEX is used to screen a library of 10^{15} random DNA sequences over many rounds of selection to obtain a single sequence that binds to the desired target with high affinity.⁵⁸ Aptamer and DNAzyme development offers the additional advantage that SELEX is performed *in vitro*, which allows aptamers to be isolated to theoretically bind any desired target, from small ions, such as Mg^{2+} or Pb^{2+} ,⁵⁹ to macromolecular proteins⁶⁰ to bacterial cells.⁶¹ Moreover, DNA molecules offer unique thermal stability in that the molecules can be denatured and renatured over several heat and cool cycles without losing its binding ability.

1.2.3.1 Aptamers

Furthermore, aptamers can easily be modified to contain the two necessary components for a biosensor: recognition element and signal transducer. The recognition element consists of a specific DNA sequence within the strand that can bind to the desired target, meanwhile the signal transducer can involve the generation of a colorimetric or fluorescent signal when the target binds to the DNA sequence. Structure-switching aptamers are particularly useful because complementary sequences labelled with a fluorophore or quencher can be hybridized to the single-stranded DNA sequence, such that fluorescence quenching occurs when no target is present, resulting in no signal production (Figure 1.3).³⁹ However, the aptamer structure changes upon the target binding, which releases the fluorophore or quencher and produces a measurable signal. Structure-switching aptamers have been developed for small molecule and protein targets, such as adenosine triphosphate (ATP) and platelet-derived growth factor (PDGF).¹⁰ The aptamers can be designed in bipartite or tripartite formats. Bipartite constructs are

composed of an aptamer strand with the fluorophore covalently linked to it and a second strand labelled with the dabcyil quencher hybridized to the aptamer. The complementary dabcyil quencher strand is designed to bind in close proximity to the fluorophore to quench fluorescence until the target is present to change the aptamer structure and release the quencher strand. The tripartite strand is composed of three strands with the fluorophore on an additional complementary strand that remains bound to the aptamer even after target addition. These fluorescence-based aptamer assays have been used in various arrangements to result in the desired output.^{15,15,56,57,60,62–65}

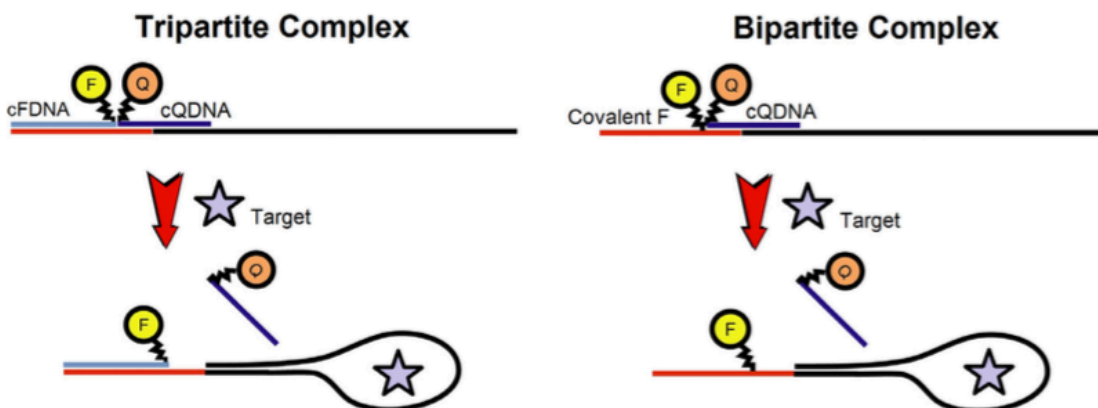


Figure 1.3. Schematic of a structure-switching aptamer in the tripartite (left) and bipartite (right) conformations. The tripartite complex is composed of three DNA strands hybridized together prior to target addition. The structure of the aptamer changes shape upon target addition and the dabcyil quencher strand (cQDNA) is released. The bipartite complex is similar to the tripartite strand, however the fluorophore is covalently linked to the aptamer strand instead. (Adapted from Carrasquilla *et al.* 2013, Ref #39).

1.2.3.2 DNAzymes

Another commonly used type of FNAs is DNAzymes, which are oligonucleotide sequences that catalyze a reaction. DNAzymes do not exist in natural systems, however ribozymes, which were discovered by Cech and Altman, are able to conduct RNA

splicing, cleavage, and peptide bond formation in ribosomes *in vivo*.^{66,67} The signal transduction element for assays using DNAzymes can involve fluorescent, colorimetric or electrochemical detection.⁵⁶ DNAzymes can also be incorporated with fluorophores and quenchers, and a catalytic reaction occurs upon target addition, which results in signal transduction.⁶⁸ There are various reactions that a DNAzyme may be capable of performing, including RNA-cleavage, DNA-cleavage, and DNA ligation reactions. DNAzymes require metal ions as cofactors for the cleavage reaction to occur, which allow them to be used as metal ion sensors. There have been DNAzymes that act in a metal dependent manner for the detection of Pb^{2+} ,⁶⁹ Zn^{2+} ,⁷⁰ Cu^{2+} ,⁷¹ and others.⁵⁹

DNA/RNA-cleaving DNAzymes cleave a specific nucleic acid sequence that acts as the substrate that triggers a catalytic reaction when the target is present.⁵⁶ The substrate can either be covalently linked to the catalytic DNAzyme (*cis*-conformation), or the substrate can be a separate strand hybridized to the DNAzyme (*trans*-conformation). Fluorescent DNAzymes are initially designed in the *cis*-conformation due to increased sensitivity, and then the *trans*-construct is designed later for applications that require the substrate to not be covalently-linked to the DNAzyme.⁷² Fluorescence as the signal transducer can be exploited by placing a fluorophore and quencher directly next to the cleavage site, such as the ribonucleotide in RNA-cleaving DNAzymes, so that either the fluorophore or quencher is released upon the target interacting with the DNAzyme (Figure 1.4).⁷³ Upon the DNAzyme cleaving the substrate strand, both the target and part of the substrate are released. Since the fluorophore and quencher are no longer in close

enough proximity for fluorescence resonance energy transfer (FRET) to occur, the fluorescent signal can be detected.

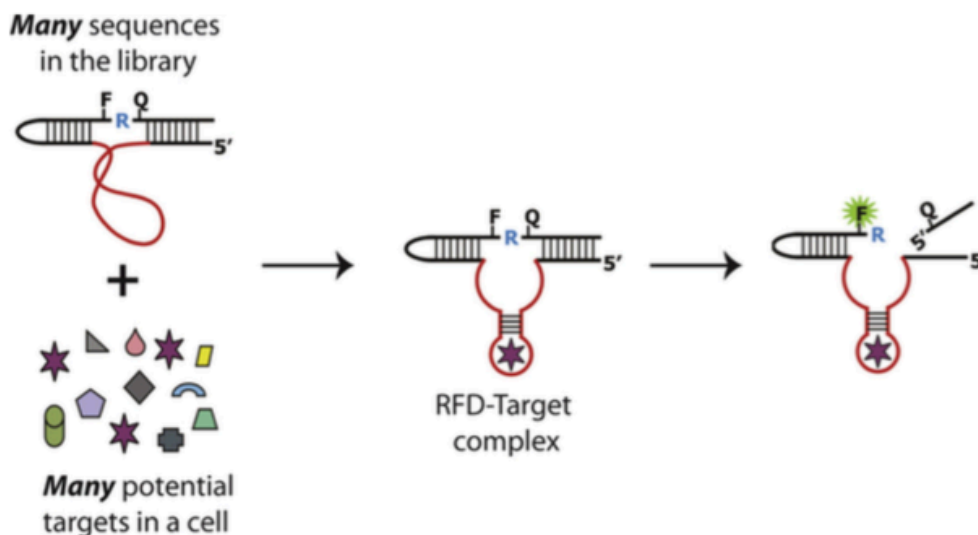


Figure 1.4. Schematic representation of the method for target binding to the DNAzyme EC1 in the *cis*-conformation. (Reproduced from Zhang *et al.* 2016, Ref # 73).

The DNAzyme EC1 is capable of *Escherichia coli* detection through the RNA-cleavage reaction of a fluorogenic substrate containing a single ribonucleotide.^{61,72–79} When the enzyme and fluorogenic substrate strands are hybridized, the presence of *E. coli* results in signal generation. The DNAzyme binds to a protein that is between 30,000 and 50,000 Da. The identity of the protein is unknown, despite the use of the DNAzyme for bacterial detection since 2011.⁶¹

1.2.3.3 FNAs in sol-gel-derived silica materials

There have been several reports of FNAs entrapped in sol-gel-derived silica materials, and it has been established that DNA aptamers, RNA aptamers, and DNAzymes respond to targets differently when entrapped in different sol-gel-derived materials.^{38,39,51} Structure-switching DNA aptamers perform optimally with SS and DGS

precursors, meanwhile RNA aptamers and DNAzymes exhibit the greatest increase in fluorescence upon target addition in 40% MTMS and 60% TMOS-derived composite material.³⁹ There are issues with biomolecule leaching from these materials, however. Notably, monomeric aptamers leached from sol-gel-derived materials more than proteins,⁸⁰ likely due to electrostatic repulsion between the anionic silica and the DNA backbone.⁵¹ The amount of DNA leaching from the material increases as the hydrophobicity and pore size of the material increases.³⁹ Similar to proteins, monomeric aptamers suffer from difficulty controlling surface chemistry and leaching.^{38,39}

1.2.4 Rolling Circle Amplification and Concatenated DNA Species

The first aptamer was isolated using *in vitro* selection in 1992 by Andrew Ellington and Jack Szostak.⁸¹ The resultant aptamers and DNAzymes that have been discovered based on *in vitro* selection first coined by Ellington and Szostak have been used as effective recognition elements in monomeric form. The small size of these FNAs is not appropriate for entrapment within macroporous sol-gel-derived materials, however.³⁹ Unlike proteins, DNA can be made into larger oligomers through a process called rolling circle amplification (RCA). Andrew Fire first published the method in 1995 and it described the DNA polymerization using the replication of short DNA circles for the enhancement of *in vitro* selection DNA libraries.⁸² The RCA process is an isothermal method to increase the size of a DNA strand by producing a long-chain of a repeating sequence.^{10,60} These RCA products, otherwise known as concatemers or amplicons, are produced by using phi29 DNA polymerase to lengthen a short DNA primer that is hybridized to a circular template that complements the monomer sequence of the FNA.

Phi29 DNA polymerase is commonly used for RCA due to its high processivity,⁸³ and the 3'→5' exonuclease activity that can be exploited in some assays.⁶⁴ RCA produces a DNA strand that can be a micrometer in length and contains hundreds or thousands of tandem repeat units.⁶⁸ The concatemers can work as efficiently as the monomer sequence, and the larger size makes the aptamers more applicable to entrapment within macroporous materials. Concatenated DNA species have been used in assays utilizing fluorescent, colorimetric, or electrochemical detection.^{11–13,56,60,84,85} In addition, RCA can be used as a signal amplification method to improve assay sensitivity in some biosensing applications.^{62,84}

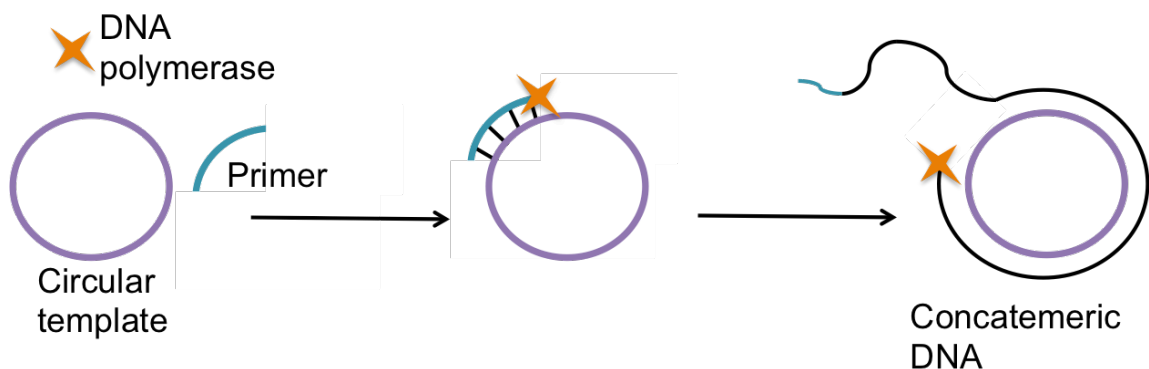


Figure 1.5. Schematic of rolling circle amplification to produce concatemeric DNA using a circular template, primer and phi29 DNA polymerase. The primer extends in the 5'→3' direction.

The size of the concatemeric DNA produced by RCA can be increased further by allowing RCA to proceed for an extended period of time in a high concentration of salt.^{15,86} The salt in the RCA buffer causes the concatemers to self-assemble into nanoflowers (Figure 1.6). The size of the nanoflowers can be tuned to be 200 nm to several micrometers in diameter depending on RCA duration.¹⁴ The self-assembly of the

nanoflowers is sequence independent because the nanoflowers do not fold based on Watson-Crick base-pairing.¹⁴ The densely-packed nanoflowers produce a larger size that may aid in material entrapment.

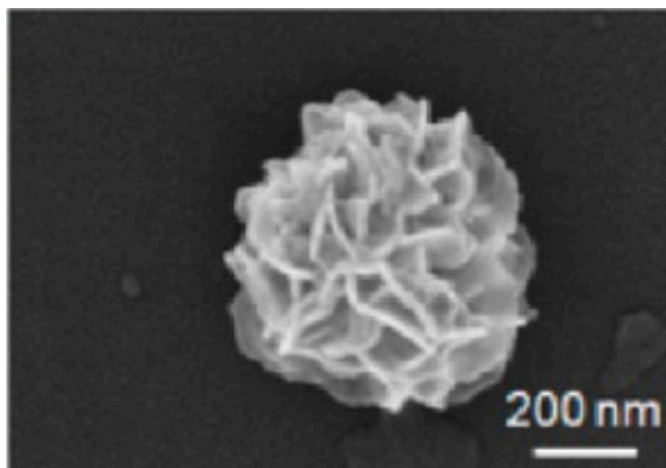


Figure 1.6. SEM image showing a typical DNA nanoflower that self-assembled after performing RCA for 10 hours. (Adapted with permission from Zhu *et al.*, Ref #15 © 2013 American Chemical Society.)

1.3 Thesis Goals

The overall goal of this thesis research was to develop monolithic biohybrid sol-gel-derived silica columns with different types of entrapped concatemeric FNAs for use as a biosensor and an affinity chromatography method that could extend the use of sol-gel entrapped biomolecules beyond the current small molecule limit. The production of long-chain FNAs utilizing RCA for amplification is an important advancement in the field that could allow FNA entrapment in sol-gel-derived silica columns. The hypothesis for this work is that DNA aptamers and DNAzymes can be concatenated for entrapment within macroporous sol-gel-derived capillary columns for protein detection.

Chapter 2 describes the development of monolithic columns with entrapped structure-switching aptamers for biosensing ATP and PDGF. This work demonstrates that monolithic sol–gel-derived silica columns can be used to detect both small molecules and macromolecular proteins. Due to the large size of concatemers, macroporous materials were able to be used for entrapment. The pores in macroporous materials are much larger, which allowed biosensing of large biomolecules such as proteins when using concatemers as the biorecognition element in columns. The concatemers entrapped within the macroporous sol–gel-derived monolithic columns provided an efficient method to create a concentration-dependent flow-based biosensor.

Chapter 3 describes the development and investigation of concatenated EC1 DNAzyme in solution. The EC1 DNAzyme responds by cleaving a fluorogenic substrate (FS28) in the presence of an unknown protein target in the crude intracellular matrix (CIM) of *E. coli*. The concatenated DNAzyme was salt aged to produce 3D DNA nanoflower superstructures, which are significantly larger and may aid in biomolecule retainment within macroporous materials in the future. The activity of the concatenated DNAzyme nanoflowers was investigated in solution. The eventual goal was to entrap the 3D nanoflowers within the materials, similar to the concatenated aptamers in Chapter 2. However, there are more challenges to overcome with the concatenated DNAzymes in solution so the sol–gel-derived material entrapment of DNAzymes was not performed.

Chapter 4 discusses the future implications of this work at the conclusion of this thesis.

1.4 References

- (1) Forsberg, E. M.; Sicard, C.; Brennan, J. D. *Annu. Rev. Anal. Chem.* **2014**, *7*, 337–359.
- (2) Cruz-Aguado, J. A.; Chen, Y.; Zhang, Z.; Brook, M. A.; Brennan, J. D. *Anal. Chem.* **2004**, *76*, 4182–4188.
- (3) Hodgson, R. J.; Chen, Y.; Zhang, Z.; Tleugabulova, D.; Long, H.; Zhao, X.; Organ, M.; Brook, M. A.; Brennan, J. D. *Anal. Chem.* **2004**, *76*, 2780–2790.
- (4) Forsberg, E. M.; Brennan, J. D. *Anal. Chem.* **2014**, *86*, 8457–8465.
- (5) Deng, N.; Liang, Z.; Liang, Y.; Sui, Z.; Zhang, L.; Wu, Q.; Yang, K.; Zhang, L.; Zhang, Y. *Anal. Chem.* **2012**, *84*, 10186–10190.
- (6) Zhao, Q.; Li, X. F.; Le, X. C. *Anal. Chem.* **2008**, *80*, 3915–3920.
- (7) Connor, A. C.; McGown, L. B. *J. Chromatogr. A* **2006**, *1111*, 115–119.
- (8) Wang, Z.; Zhao, J. C.; Lian, H. Z.; Chen, H. Y. *Talanta* **2015**, *138*, 52–58.
- (9) Zhao, Q.; Li, X. F.; Shao, Y.; Le, X. C. *Anal. Chem.* **2008**, *80*, 7586–7593.
- (10) Carrasquilla, C.; Little, J. R. L.; Li, Y.; Brennan, J. D. *Chem. Eur. J.* **2015**, *21*, 7369–7373.
- (11) Cheglakov, Z.; Weizmann, Y.; Basnar, B.; Willner, I. *Org. Biomol. Chem.* **2007**, *5*, 223–225.
- (12) Cheglakov, Z.; Weizmann, Y.; Braunschweig, A. B.; Wilner, O. I.; Willner, I. *Angew. Chemie - Int. Ed.* **2008**, *47*, 126–130.
- (13) Wang, F.; Lu, C. H.; Liu, X.; Freage, L.; Willner, I. *Anal. Chem.* **2014**, *86*, 1614–1621.

- (14) Lv, Y.; Hu, R.; Zhu, G.; Zhang, X.; Mei, L.; Liu, Q.; Qiu, L.; Wu, C.; Tan, W. *Nat. Protoc.* **2015**, *10*, 1508–1524.
- (15) Zhu, G.; Hu, R.; Zhao, Z.; Chen, Z.; Zhang, X.; Tan, W. *J. Am. Chem.* **2013**, *135*, 1–10.
- (16) Avnir, D.; Braun, S.; Lev, O.; Ottolenghi, M. *Chem. Mater.* **1994**, *6*, 1605–1614.
- (17) Gill, I. *Chem. Mater.* **2001**, *13*, 3404–3421.
- (18) Pfaunmiller, E. L.; Hartmann, M.; Dupper, C. M.; Soman, S.; Hage, D. S. *J. Chromatogr. A* **2012**, *1269*, 198–207.
- (19) Besanger, T. R.; Hodgson, R. J.; Green, J. R. A.; Brennan, J. D. *Anal. Chim. Acta* **2006**, *564*, 106–115.
- (20) Chen, Y.; Wu, M.; Wang, K.; Chen, B.; Yao, S.; Zou, H.; Nie, L. *J. Chromatogr. A* **2011**, *1218*, 7982–7988.
- (21) Karwa, M.; Hahn, D.; Mitra, S. *Anal. Chim. Acta* **2005**, *546*, 22–29.
- (22) Monton, M. R. N.; Forsberg, E. M.; Brennan, J. D. *Chem. Mater.* **2012**, *24*, 796–811.
- (23) Tudorache, M.; Bala, C. *Anal. Bioanal. Chem.* **2007**, *388*, 565–578.
- (24) Brennan, J. D. *Acc. Chem. Res.* **2007**, *40*, 827–835.
- (25) Braun, S.; Rappoport, S.; Zusman, R.; Avnir, D.; Ottolenghi, M. *Mater. Lett.* **1990**, *10*, 1–5.
- (26) Gill, I.; Ballesteros, A. *J. Am. Chem. Soc.* **1998**, *120*, 8587–8598.
- (27) Gill, I.; Ballesteros, A. *Trends Biotechnol.* **2000**, *18*, 282–296.
- (28) Avnir, D.; Coradin, T.; Lev, O.; Livage, J. *J. Mater. Chem.* **2006**, *16*, 1013–1030.

- (29) Frenkel-Mullerad, H.; Avnir, D. *J. Am. Chem. Soc.* **2005**, *127*, 8077–8081.
- (30) Walcarius, A.; Collinson, M. M. *Annu. Rev. Anal. Chem.* **2009**, *2*, 121–143.
- (31) Dave, B. C.; Soyez, H.; Miller, J. M.; Dunn, B.; Valentine, J. S.; Zink, J. I. *Chem. Mater.* **1995**, *7*, 1431–1434.
- (32) Yi, Y.; Chen, Y.; Brennan, J. D.; Brook, M. A. *Chem. Mater.* **2006**, *18*, 5336–5342.
- (33) Amoura, M.; Nassif, N.; Roux, C.; Livage, J.; Coradin, T. *Chem. Commun.* **2007**, No. 39, 4015–4017.
- (34) Liu, B.; Cao, Y.; Chen, D.; Kong, J.; Deng, J. *Anal. Chim. Acta* **2003**, *478*, 59–66.
- (35) Bhatia, R. B.; Brinker, C. J.; Gupta, A. K.; Singh, A. K. *Chem. Mater.* **2000**, *12*, 2434–2441.
- (36) Besanger, T. R.; Brennan, J. D. *J. Sol-Gel Sci. Technol.* **2006**, *40*, 209–225.
- (37) Brook, M. A.; Chen, Y.; Guo, K.; Zhang, Z.; Jin, W.; Deisingh, A.; Cruz-Aguado, J.; Brennan, J. D. *J. Sol-Gel Sci. Technol.* **2004**, *31*, 343–348.
- (38) Hui, C. Y.; Li, Y.; Brennan, J. D. *Chem. Mater.* **2014**, *26*, 1896–1904.
- (39) Carrasquilla, C.; Brennan, J. D. *Methods* **2013**, *63*, 255–265.
- (40) Dong, H.; Brennan, J. D. *Chem. Mater.* **2006**, *18*, 4176–4182.
- (41) Dong, H.; Brennan, J. D. *J. Colloid Interface Sci.* **2015**, *437*, 50–57.
- (42) Dong, H.; Brennan, J. D. *J. Mater. Chem.* **2012**, *22*, 13197.
- (43) Jin, W.; Brennan, J. D. *Anal. Chim. Acta* **2002**, *461*, 1–36.
- (44) Nakanishi, K. *J. Porous Mater.* **1997**, *4*, 67–112.
- (45) Feinle, A.; Elsaesser, M. S.; Hüsing, N. *Chem. Soc. Rev.* **2016**, *45*, 3377–3399.

- (46) Ishizuka, N.; Minakuchi, H.; Nakanishi, K.; Hirao, K.; Tanaka, N. *Colloids Surfaces A Physicochem. Eng. Asp.* **2001**, *187–188*, 273–279.
- (47) Moaddel, R.; Wainer, I. W. *Nat. Protoc.* **2009**, *4*, 197–205.
- (48) Besanger, T. R.; Chen, Y.; Deisingh, A. K.; Hodgson, R.; Jin, W.; Mayer, S.; Brook, M. A.; Brennan, J. D. *Anal. Chem.* **2003**, *75*, 2382–2391.
- (49) Sharma, J.; Besanger, T. R.; Brennan, J. D. *Anal. Chem.* **2008**, *80*, 3213–3220.
- (50) Hodgson, R. J.; Besanger, T. R.; Brook, M. A.; Brennan, J. D. *Anal. Chem.* **2005**, *77*, 7512–7519.
- (51) Rupcich, N.; Nutiu, R.; Li, Y.; Brennan, J. D. *Anal. Chem.* **2005**, *77*, 4771–4778.
- (52) Besanger, T. R.; Easwaramoorthy, B.; Brennan, J. D. *Anal. Chem.* **2004**, *76*, 6470–6475.
- (53) Forsberg, E. M.; Green, J. R. A.; Brennan, J. D. *Anal. Chem.* **2011**, *83*, 5230–5236.
- (54) Lebert, J. M.; Forsberg, E. M.; Brennan, J. D. *Biochem. Cell Biol.* **2008**, *86*, 100–110.
- (55) Kovarik, P.; Hodgson, R. J.; Covey, T.; Brook, M. A.; Brennan, J. D. *Anal. Chem.* **2005**, *77*, 3340–3350.
- (56) Liu, J.; Cao, Z.; Lu, Y. *Chem. Rev.* **2009**, *109*, 1948–1998.
- (57) Brody, E. N.; Willis, M. C.; Smith, J. D.; Jayasena, S.; Zichi, D.; Gold, L. *Mol. Diagnosis* **1999**, *4*, 381–388.
- (58) Wilson, D. S.; Szostak, J. W. *Annu. Rev. Biochem.* **1999**, *68*, 611–647.
- (59) Shen, Y.; Mackey, G.; Rupcich, N.; Gloster, D.; Chiuman, W.; Li, Y.; Brennan, J. D. *Anal. Chem.* **2007**, *79*, 3494–3503.

- (60) Zhao, W.; Ali, M. M.; Brook, M. A.; Li, Y. *Angew. Chemie - Int. Ed.* **2008**, *47*, 6330–6337.
- (61) Ali, M. M.; Aguirre, S. D.; Lazim, H.; Li, Y. *Angew. Chemie - Int. Ed.* **2011**, *50*, 3751–3754.
- (62) Liu, M.; Hui, C. Y.; Zhang, Q.; Gu, J.; Kannan, B.; Jahanshahi-Anbuhi, S.; Filipe, C. D. M.; Brennan, J. D.; Li, Y. *Angew. Chemie - Int. Ed.* **2016**, *55*, 2709–2713.
- (63) Zhao, Q.; Wu, M.; Chris Le, X.; Li, X. F. *TrAC - Trends Anal. Chem.* **2012**, *41*, 46–57.
- (64) Liu, M.; Zhang, W.; Zhang, Q.; Brennan, J. D.; Li, Y. *Angew. Chemie - Int. Ed.* **2015**, *54*, 9637–9641.
- (65) Lv, Y.; Hu, R.; Zhu, G.; Zhang, X.; Mei, L.; Liu, Q.; Qiu, L.; Wu, C.; Tan, W. *Nat Protoc* **2015**, *10* (10), 1508–1524.
- (66) Kruger, K.; Grabowski, P. J.; Zaug, A. J.; Sands, J.; Gottschling, D. E.; Cech, T. R. *Cell* **1982**, *31*, 147–157.
- (67) Guerrier-Takada, C.; Gardiner, K.; Marsh, T.; Pace, N.; Altman, S. *Cell* **1983**, *35*, 849–857.
- (68) Wang, F.; Lu, C. H.; Willner, I. *Chem. Rev.* **2014**, *114*, 2881–2941.
- (69) Brown, A. K.; Li, J.; Pavot, C. M. B.; Lu, Y. *Biochemistry* **2003**, *42*, 7152–7161.
- (70) Santoro, S. W.; Joyce, G. F.; Sakthivel, K.; Gramatikova, S.; Barbas, C. F. *J. Am. Chem. Soc.* **2000**, *122*, 2433–2439.
- (71) Carmi, N.; Balkhi, S. R.; Breaker, R. R. *Proc. Natl. Acad. Sci. U. S. A.* **1998**, *95*, 2233–2237.

- (72) Aguirre, S. D.; Ali, M. M.; Salena, B. J.; Li, Y. *Biomolecules* **2013**, *3*, 563–577.
- (73) Zhang, W.; Feng, Q.; Chang, D.; Tram, K.; Li, Y. *Methods* **2016**, *106*, 66–75.
- (74) Tram, K.; Kanda, P.; Salena, B. J.; Huan, S.; Li, Y. *Angew. Chemie - Int. Ed.* **2014**, *53*, 12799–12802.
- (75) Ali, M.; Aguirre, S. D.; Mok, W. W. K.; Li, Y. *Methods Mol. Biol.* **2012**, *848*, 395–418.
- (76) Aguirre, S. D.; Ali, M. M.; Kanda, P.; Li, Y. *J. Vis. Exp.* **2012**, *63*, 1–7.
- (77) Tram, K.; Kanda, P.; Li, Y. *J. Nucleic Acids* **2012**, *2012*, 1–8.
- (78) Qu, L.; Ali, M. M.; Aguirre, S. D.; Liu, H.; Jiang, Y.; Li, Y.; Leng, F. *PLoS One* **2014**, *9*, 1–17.
- (79) Shen, Z.; Wu, Z.; Chang, D.; Zhang, W.; Tram, K.; Lee, C.; Kim, P.; Salena, B. J.; Li, Y. *Angew. Chemie - Int. Ed.* **2016**, *55*, 2431–2434.
- (80) Zheng, L.; Reid, W. R.; Brennan, J. D. *Anal. Chem.* **1997**, *69*, 3940–3949.
- (81) Ellington, A. D.; Szostak, J. W. *Nature* **1992**, *355*, 850–852.
- (82) Fire, A.; Xu, S. Q. *Proc. Natl. Acad. Sci.* **1995**, *92*, 4641–4645.
- (83) Kamtekar, S.; Berman, A. J.; Wang, J.; Vega, M. De; Blanco, L.; Salas, M.; Steitz, T. A. *Mol. Cell* **2004**, *16*, 609–618.
- (84) Liu, M.; Zhang, Q.; Li, Z.; Gu, J.; Brennan, J. D.; Li, Y. *Nat Commun* **2016**, *7*, 12074–12080.
- (85) Liu, M.; Zhang, Q.; Chang, D.; Gu, J.; Brennan, J. D.; Li, Y. *Angew. Chemie* **2017**, *56*, 6142–6146.
- (86) Hu, R.; Zhang, X.; Zhao, Z.; Zhu, G.; Chen, T.; Fu, T.; Tan, W. *Angew. Chemie -*

M.Sc. Thesis – E.Q. Kapteyn – McMaster University – Chemical Biology

Int. Ed. **2014**, 53, 5821–5826.

CHAPTER 2 | SOL-GEL DERIVED BIOHYBRID MATERIALS INCORPORATING LONG-CHAIN DNA APTAMERS

The following chapter was published in the journal *Angewandte Chemie International Edition* under the following citation:

Carrasquilla, C., Kapteyn, E., Li, Y., Brennan, J.D., **Sol-Gel Derived Biohybrid Materials Incorporating Long-Chain DNA Aptamers**, *Angewandte Chemie Int. Ed.*, **2017**, 56(36), 10686-10690.

Carmen Carrasquilla and the author fabricated the columns and performed the flow-based column assays. The author performed SEM imaging, EDX analysis of the monolithic sol-gel-derived silica capillary columns, and column assays present in the appendix. Additionally, the author and Carmen Carrasquilla both performed column fabrication, fraction collection, and column assays. Carmen Carrasquilla performed the majority of the other experiments, including the materials assay screen and the majority of the data analysis. The final manuscript was written by Carmen Carrasquilla, Dr. Li, and Dr. Brennan. This article was printed with permission from John Wiley and Sons ©. The electronic supporting information is included as the Appendix at the end of this chapter.

2.1 Abstract

Sol-gel derived bio/inorganic hybrid materials have been examined for diverse applications, including biosensing, affinity chromatography and drug discovery. However, such materials have mostly been restricted to the interaction between entrapped biorecognition elements and small molecules, owing to the requirement for nanometer-scale mesopores in the matrix to retain entrapped biorecognition elements. Herein, we report on a new class of macroporous bio/inorganic hybrids, engineered through a high-throughput materials screening approach, that entrap micron-sized concatemeric DNA aptamers. We demonstrate that the entrapment of these long-chain DNA aptamers allows their retention within the macropores of the silica material, so that aptamers can interact with high molecular weight targets such as proteins. Our approach overcomes the major limitation of previous sol-gel derived biohybrid materials by enabling molecular recognition for targets beyond small molecules.

2.2 Introduction

The sol-gel process has been widely used to entrap molecular recognition elements (MREs) into porous materials to produce various analytical devices.¹⁻⁷ In all cases, the retention of entrapped MREs was based on size exclusion and required materials with mesopore diameters of under 10 nm. As such, these hybrid materials were restricted to interactions with molecules less than 2 kDa,⁸ as larger targets were unable to access the entrapped MREs.⁹⁻¹⁵

To extend this approach to larger analytes, it is necessary to produce materials with macroporous morphologies. To prevent leaching of MREs, it is possible to immobilize them to the surface of the material using covalent or affinity-based interactions.¹⁶⁻²⁰ However, these methods require multiple time-consuming steps, can lead to MRE denaturation, and have lower loading capacity compared to sol-gel entrapment. An alternative method, which has not been reported before, is the entrapment of MREs that are large enough to remain immobilized even in micron-sized pores. In such a case, these micron-size MREs should remain accessible to large analytes, allowing for a major expansion in the utility of sol-gel derived biohybrids. This led us to investigate the entrapment of concatemeric DNA aptamers as the MRE, which can be easily produced by rolling circle amplification (RCA).

RCA is a biochemical reaction in which a DNA polymerase makes repeated copies of a circular single-stranded (ss) DNA template to produce very large ss DNA amplicons that contain a repetitive sequence.^{21,22} Importantly, there is no restriction on the length of circular template (RCA has been used to amplify the genome of M13 phage^{23,24}), and the

amplicons can reach megadalton molecular weights (MW).^{25,26} When the circular DNA template is designed to contain the complementary sequence of a DNA aptamer, its RCA reaction will generate long strands of DNA containing tandem aptameric repeats,²⁷ which are referred to as concatemeric DNA aptamers in this report. Herein, we demonstrate that concatemeric aptamers can be entrapped into specially-designed macroporous sol-gel derived organosilicate composites with high target-binding activity and minimal leaching, allowing for fabrication of flow-through biosensors to detect both small and large targets.

Our initial goal was to identify an appropriate porous material for entrapping concatemeric aptamers. The morphology of sol-gel materials is affected by several parameters that control gelation time and phase separation, which include types of silica precursors and porogens, reaction pH and ionic strength.^{9,11,28} For this reason, we adapted a previously reported screening approach²⁸ to identify suitable compositions that could retain concatemeric aptamers with minimal leaching, allow concatemer accessibility to both small-molecule and protein targets, produce self-supporting monolithic capillary columns, and allow pressure-driven flow through a capillary column with low backpressure.

2.3 Results and Discussion

A total of 140 formulations were prepared from four silica precursors – sodium silicate (SS), tetramethoxysilane (TMOS), methyltrimethoxysilane (MTMS) or 40 vol% MTMS in TMOS, which were previously used for entrapping functional aptamers (see Appendix for experimental detail).²⁹ Each precursor was combined with five

concentrations (0, 1.25, 2.5, 5, 10% w/v) of seven poly(ethylene glycol) (PEG) species varying in MW. Macroporosity was assessed by measuring the transmittance of each material at 400 nm, which decreases owing to increased light scattering as materials become more macroporous (Figure S2.1). We selected a cutoff of 20% transmittance, below which materials were considered to be macroporous.²⁸ Figure 2.1 demonstrates that transmittance (and hence morphology) can be carefully controlled by adjusting the precursor and porogen properties. Many materials comprised of SS, TMOS or 40 vol% MTMS in TMOS with variable amounts of PEG demonstrated transmittance values indicative of macroporosity and formed self-supporting monoliths without flocculation, and thus were further investigated.

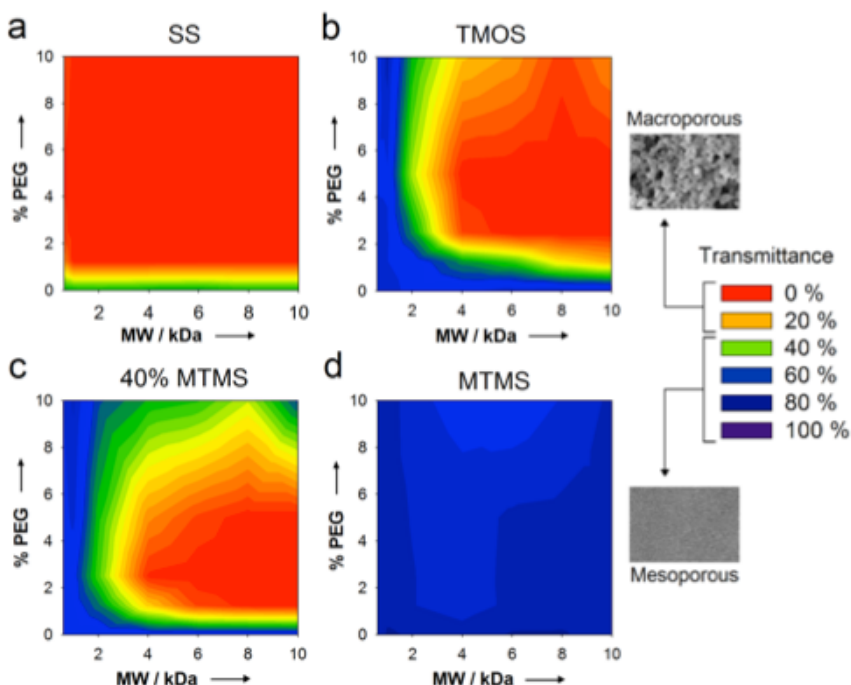


Figure 2.1. Opacity plots of sol-gel derived materials. Percent transmittance of a) SS, b) TMOS, c) 40% TMMS (in TMOS), and d) MTMS sols mixed in assay buffer with 0 – 10 kDa PEG at various concentrations after 3 h gelation at room temperature. Materials with transmittance $\leq 20\%$ are considered to be macroporous.

Two structure-switching DNA aptamers were chosen for this study, one for adenosine triphosphate (ATP), and another for the platelet-derived growth factor (PDGF) protein^{30,31} (see Table S1 for the DNA sequences used).^{32–34} In this design, fluorophore and quencher-labeled DNA strands (FDNA and QDNA, respectively) hybridize to the monomeric or concatemeric aptamers to form a quenched aptamer/DNA duplex. Upon binding its target, this duplex undergoes a conformational change to release the QDNA and produce a fluorescence signal enhancement. Dynamic light scattering measurements of monomeric and concatemeric aptamers in solution (Figure S2.2) demonstrated that the average hydrodynamic diameter of the concatemeric aptamers was $\sim 1.5 \mu\text{m}$, which was much higher than the size of monomeric aptamers ($\sim 20 \text{ nm}$ if fully extended). The small peak at $\sim 100 \text{ nm}$ comes from the circular DNA template.

We examined the effect of PEG on the structure-switching ability of aptamers in solution, as it was reported that high levels of PEG can prevent hybridization of FDNA and QDNA with the aptamers.^{35,36} Figure S2.3 demonstrates that reduced signal enhancement occurs with increasing concentration and MW of PEG. Therefore, a subset of 24 macroporous materials, with low to intermediate MWs and concentrations of PEG, were chosen for aptamer entrapment (Table S2.2).

Figure 2.2 shows the leaching of entrapped monomeric and concatemeric aptamers, as determined by the fluorescence intensity of the supernatant used to wash the monoliths. Monomeric aptamers demonstrated substantial leaching from mesoporous materials (50%) and almost complete leaching from macroporous materials (90%), showing that leaching increases with pore size. Conversely, concatemeric aptamers demonstrated

significantly lower leaching from all materials (20% or less) due to their larger size relative to monomers, and fluorescence polarization studies revealed that the intensity arose from dehybridized FDNA rather than loss of concatemeric aptamers (Table S2.3), indicating efficient entrapment of concatemeric aptamers in macroporous materials. Based on these results, further studies focused on a subset of three macroporous materials: SS with 5% of 0.6 kDa PEG (Macro SS), TMOS with 5% 6 kDa PEG (Macro TMOS), and 40% MTMS with 5% 6 kDa PEG (Macro 40% MTMS). Corresponding mesoporous materials were also tested, which had identical precursor compositions but lacked PEG.

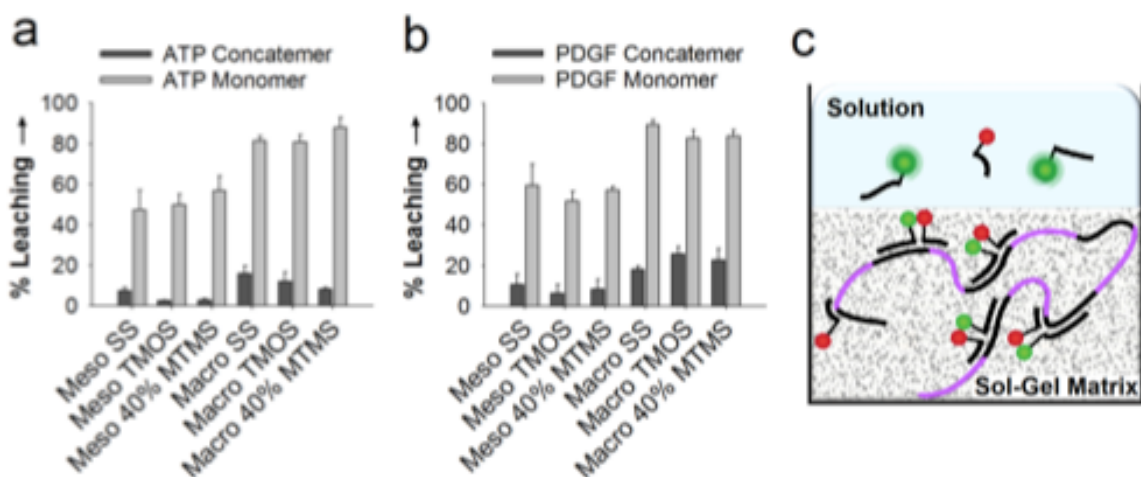


Figure 2.2. Aptamer leaching from sol-gel derived materials. The percent leaching of a) ATP concatemers versus monomers and b) PDGF concatemers versus monomers entrapped in various mesoporous or macroporous sol-gel derived materials. C) schematic of concatemers entrapped within a macro porous matrix.

We next evaluated signal response of entrapped monomeric and concatemeric aptamers when exposed to their cognate targets (2 mM ATP or 200 nM PDGF), which would depend on both access of the analyte to the entrapped aptamer and the ability of the

aptamer to retain structure-switching ability. In mesoporous materials, both monomeric and concatemeric versions of the ATP aptamer showed a similar response to ATP (~8–10-fold increase in signal, Fig. 2.3A) while addition of PDGF to entrapped monomeric and concatemeric PDGF aptamers produced no increase in fluorescence (Fig. 2.3B), indicating that the PDGF was unable to enter the mesoporous material, as expected. However, macroporous materials containing concatemeric aptamers demonstrated substantial fluorescence enhancements, with an 8-fold enhancement for the ATP aptamer (Fig. 2.3A) and up to a 3-fold enhancement for the PDGF aptamer (Fig. 2.3B). In stark contrast, addition of cognate targets to macroporous materials containing monomeric aptamers produced much lower fluorescence enhancements, consistent with loss of the entrapped aptamers via leaching, while addition of unintended targets to entrapped concatemeric aptamers produced no signal (Figure S3.4), demonstrating retention of the expected selectivity. These results conclusively demonstrate that entrapment of long-chain DNA aptamers in optimized macroporous materials allows detection of targets spanning small molecules to proteins.

We also examined concentration-dependent signal responses of concatemeric ATP (Figure 2.3C) and PDGF (Figure 2.3D) aptamers entrapped in Meso and Macro 40% MTMS. While ATP could induce a concentration-dependent fluorescence enhancement in both materials, PDGF was only able to cause a signal change in the macroporous material, further confirming that large targets such as PDGF require macropores to access the entrapped aptamers. Interestingly, while aptamers remained accessible to proteins, their entrapment within macropores did afford some protection against degradation by

nucleases (>60 min for full degradation when entrapped vs. ~1 min in solution, Figure S2.5), demonstrating another advantage of these materials. Inclusion of nuclease inhibitors into samples should further reduce nuclease degradation.

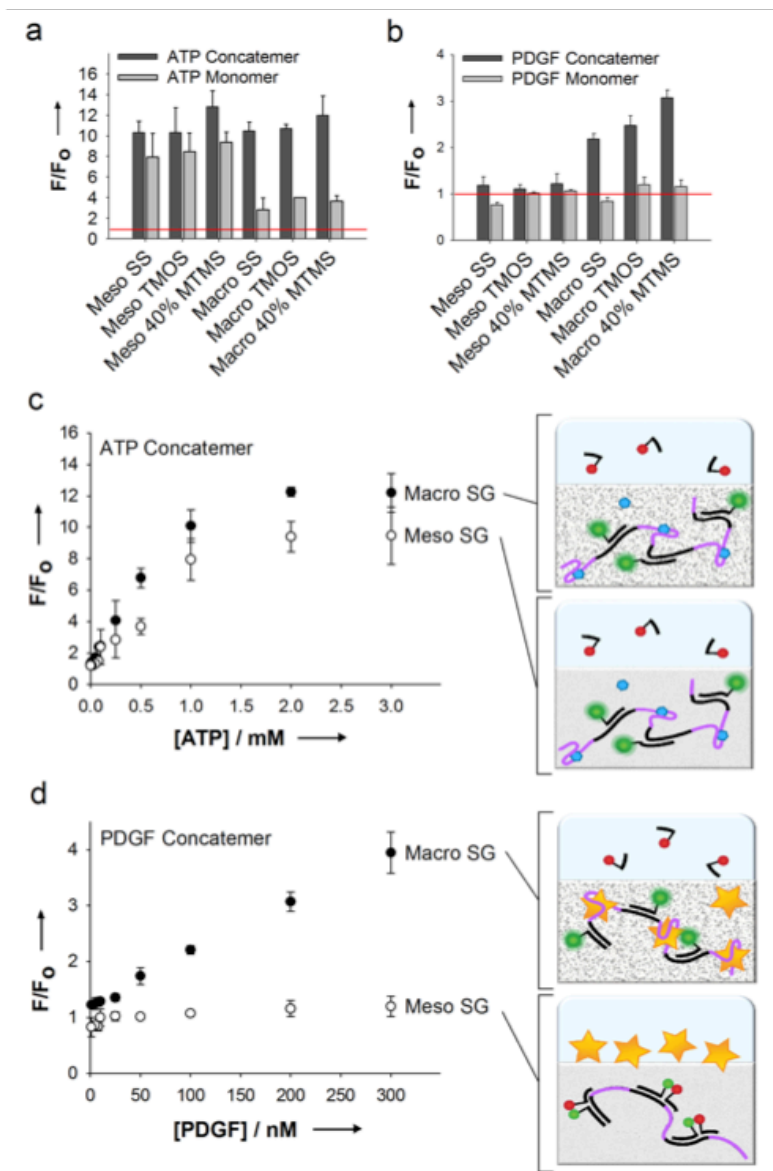


Figure 2.3. Signal response comparison of aptamer reporters. Fluorescence from a) ATP-binding monomer and concatemer with 2 mM ATP or b) PDGF-binding monomer and concatemer with 200 nM PDGF in various mesoporous or macroporous materials. The red line in a) and b) indicates a normalized F/F_0 of 1.0 (no signal increase). Response of c) ATP-binding concatemer with 0 – 3 mM ATP or d) PDGF-binding concatemer with 0 – 300 nM PDGF in Meso or Macro 40% MTMS.

As a practical demonstration of the utility of the macroporous materials, we produced aptamer-doped monolithic columns within fused silica capillaries using the 40% MTMS material for use as flow-through biosensors. The columns could withstand flow rates up to 30 $\mu\text{L}/\text{min}$, though at very high backpressures, but were typically utilized at a flow rate of 1 $\mu\text{L}/\text{min}$, which allowed operation at a low backpressure (Figure S2.6). Scanning electron microscopy (SEM) was used to image the structure of monolithic columns with and without entrapped concatemeric aptamers (Figure 2.4). Undoped columns showed macropores on the order of 1 – 2 μm in diameter. Columns with concatemeric aptamers showed a substantially different structure, with the appearance of roughly spherical DNA structures coating the silica particles. Energy dispersive x-ray spectroscopy (EDX) was used to compare the elemental composition of columns with or without entrapped concatemers (Figure S2.7). In columns containing concatemeric aptamers, the decreased contribution from silicon and increased carbon and nitrogen content support the conclusion that the nanostructures observed using SEM are in fact long-chain DNA aptamers coating the silica skeleton.

Taken together, the SEM and EDX data show that the aptamers are likely adsorbed or partially entrapped in the materials, with a significant amount of the concatemer exposed to the pore solvent. Previous fluorescence studies of entrapped aptamers³⁷ show that aptamers remain highly mobile when entrapped, indicating that the anionic DNA is not strongly adsorbed to either silica or organosilicate surfaces, and thus retains structure-switching ability. Thus, the aptamers are likely retained primarily as a result of size exclusion, where large concatemers are simply too big to elute even through micron scale

pores.

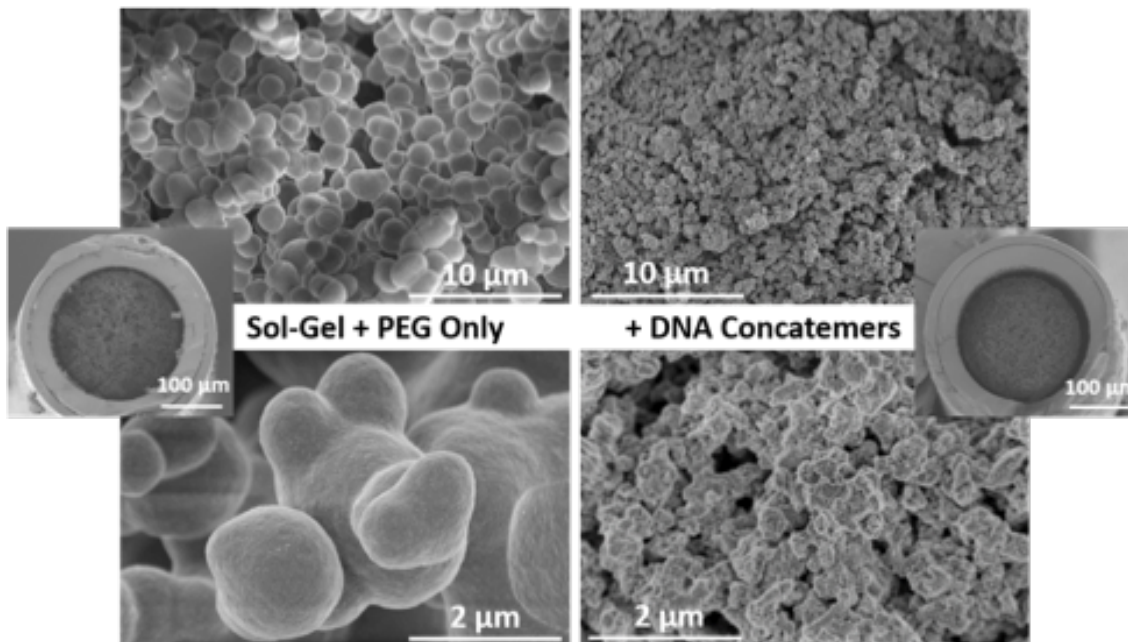


Figure 2.4. SEM images of sol-gel derived monolithic columns. Magnified images of a monolithic column with or without entrapped concatemeric aptamers formed in a 250 µm i.d. capillary using SEM analysis of non-conductive materials.

To achieve flow-through sensing, the quencher in the QDNA strand was replaced with a fluorophore (FAM or Cy5) to produce F'DNA, and the original FDNA was not included. In this configuration, the F'DNA is released upon target binding and produces a fluorescence spike upon elution (Figure 2.5A). Upon addition of cognate target, the column eluate showed a concentration-dependent fluorescence increase (Figure S2.8) for both ATP (Figure 2.5B) and PDGF (Figure 2.5C) systems, while addition of targets to columns with entrapped monomers or F'DNA alone resulted in no fluorescence (Figure 2.5B and 2.5C, insets). PDGF could also be detected when present in blood serum (Figure S2.9) and the columns could be used to entrap both concatemeric aptamers simultaneously (PDGF—FAM and ATP-Cy5) for multiplexed detection (Figure S2.10).

Hence, the entrapment of concatemeric aptamers into macroporous columns enables fabrication of flow-based sensors for a range of targets, and should also be amenable to affinity based purification or evaluation of aptamer-target binding constants using well known chromatographic methods.^{38–41}

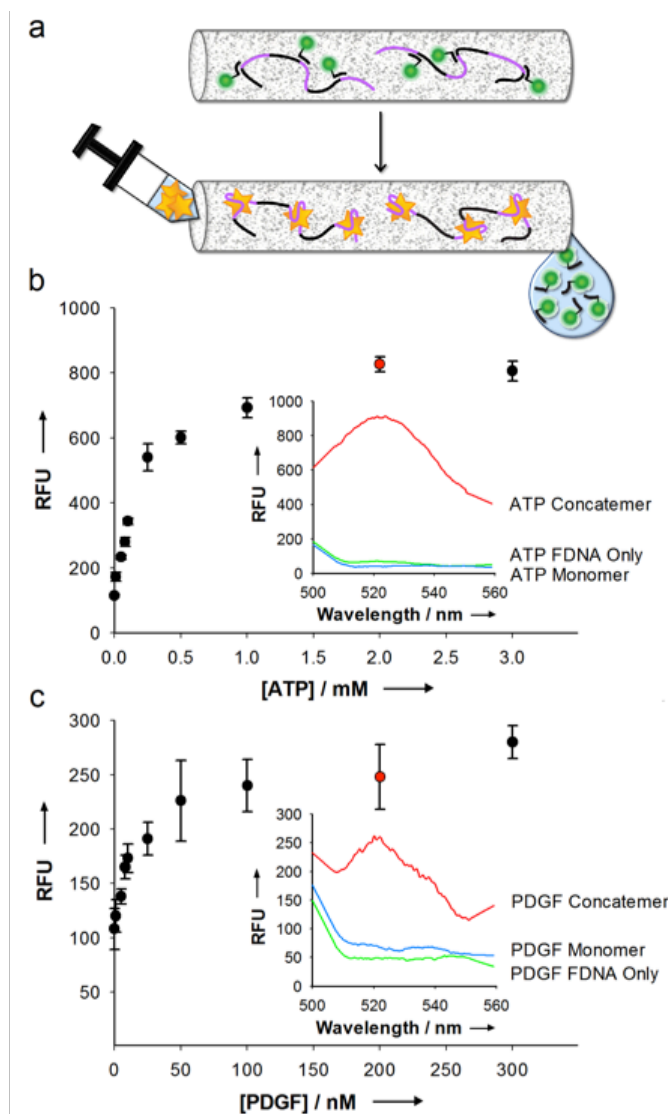


Figure 2.5. Target detection using aptameric monolithic columns. A) Schematic of macroporous sol-gel derived monolith containing concatemeric aptamers and target binding-induced release of F'DNA. B) ATP concatemer column response to 0 – 300 nM PDGF. Insets: representative fluorescence scans of eluate fractions upon target addition – b) 2 mM ATP or c) 200 nM PDGF.

2.4 Conclusions

In conclusion, we have shown that concatemeric DNA aptamers produced by RCA can be entrapped and retained within macroporous sol-gel derived materials with minimal leaching, high activity and the ability to bind high MW targets. This work also demonstrates that screening of sol-gel derived materials offers an efficient way to identify a macroporous material that can retain aptamer functionality and allow fabrication of monolithic capillary columns, which can be used as flow-based biorecognition columns. This work expands the use of sol-gel entrapped biomolecules beyond small targets toward large macromolecules such as proteins, enabling multiple new applications of sol-gel derived bio/inorganic hybrid materials.

2.5 Experimental Section

2.5.1 Materials. Standard and functionalized DNA oligonucleotides were synthesized and purified by HPLC by Integrated DNA Technologies (Coralville, IA). Adenosine 5'-triphosphate (ATP), cytidine 5'-triphosphate (CTP), guanosine 5'-triphosphate (GTP), uridine 5'-triphosphate (UTP), deoxyribonuclease I (DNase I), T4 polynucleotide kinase (PNK; with 10× reaction buffer A), T4 DNA ligase (with 10× T4 DNA ligase buffer), 10 mM dNTPs, phi29 DNA polymerase (with 10× phi29 DNA polymerase buffer), GeneRuler™ 1 kb Plus DNA ladder and 10,000× SYBR Safe DNA gel stain were purchased from Fermentas Life Sciences (Burlington, ON). Recombinant human platelet derived growth factor (PDGF), epidermal growth factor (EGF) and insulin-like growth factor I (IGF-I) were purchased from Cedarlane (Burlington, ON). Sodium silicate

solution (SS solution, ultrapure grade, ~14% Na₂O, ~29% silica) was purchased from Fisher Scientific (Pittsburgh, PA). Human serum (sterile-filtered from male AB clotted whole blood), bovine serum albumin (BSA), poly(ethylene) glycol (PEG, 600 – 10,000 Da), tetramethoxysilane (TMOS), methyltrimethoxysilane (MTMS), and Dowex 50x8–100 cation exchange resin and all other analytical grade chemicals and solvents were purchased from Sigma-Aldrich (Oakville, ON). Water was purified prior to use with a Millipore Milli-Q Synthesis A10 water purification system.

2.5.2 Methods.

Preparation of Concatemeric DNA Aptamers and Reporter Complexes. Concatemer constructs of each structure-switching aptamer and the fluorescence-signaling aptamer reporter complexes for ATP and PDGF binding were prepared using the sequences given in Table S1 as described elsewhere²⁷ and briefly below. The linear circular templates were first phosphorylated using 10 U of T4 PNK and 100 nmol ATP at 37 °C for 30 min followed by heating at 90 °C for 5 min and cooling to room temperature. These were then ligated using 15 U of T4 DNA ligase at room temperature for 12 h in 1× ligase buffer. The circularized templates were ethanol precipitated before purifying on a 10% polyacrylamide gel, ethanol precipitated and resuspended in water.

The RCA reaction of each aptamer sequence was carried out by heating 10 pmol of circular template with 10 pmol of primer and 5 µL of 10× phi29 polymerase buffer (36.5 µL total volume) at 90 °C for 1 min. Following cooling, 2.5 µL of 10 µM dNTPs and 10

U of phi29 polymerase were added to the reaction mixture and allowed to incubate at 30 °C for 1 h. The reaction was followed by a 5-fold dilution with water before heating at 90 °C for 5 min to deactivate the enzyme. The concatemeric aptamers from the reaction mixture were purified by centrifugation using a 100 kDa Nanosep[®] spin column and quantified using a NanoVue spectrophotometer (absorbance at 260 nm). As the exact size of the concatemer construct is unknown, its approximate molar concentration was obtained based on one repeat of the monomeric aptamer sequence.

Tripartite reporter complexes were prepared by combining either the concatemeric or monomeric aptamer with its FDNA and QDNA in a 1:1:6 molar ratio (100 nM final concentration of FDNA), respectively, in assay buffer (40 mM Tris·HCl, 200 mM NaCl, 4 mM MgCl₂ at pH 7.8). Our previous work determined that using a 1:1 aptamer/FDNA ratio with 6× QDNA produced the greatest amount of quenching for low initial background fluorescence prior to target binding and a sensitivity and selectivity similar to the monomeric aptamer reporter systems.²⁷ These solutions were then heated at 90 °C for 5 minutes, cooled and incubated for 30 minutes at room temperature.

Optimization of Concatemer Fluorescence Signaling in Solution. To study the effects of PEG on signaling in solution, the reporter system solutions were prepared at 2× concentration then mixed in a 1:1 ratio with 1.25 – 10% PEG (w/v, final) of 4 – 10 kDa. Baseline fluorescence was measured for 10 min prior to the addition of target. Target

analyte for each aptamer was then added at a final concentration of 2 mM ATP or 200 nM PDGF to the appropriate system and fluorescence measurements were continued.

Preparation of Sols and Monolithic Silica Disks. The silica and organosilicate precursors SS, TMOS and MTMS, were used to prepare the sols for aptamer entrapment studies as described elsewhere.²⁹ Sodium silicate sols were prepared by diluting 2.59 g of a stock SS solution to 10 mL with water, mixing the solution with 5.5 g DOWEX for 2 min to bring the pH to ~4, and then vacuum filtering this solution through a Büchner funnel to remove the resin followed by further filtration through a 0.2 µm membrane syringe filter to remove any particulates in the solution. Before use, 120 g of the Dowex resin was cleaned by stirring in 150 mL 0.1 N HCl for 1 h, followed by vacuum filtration and washing with water until the filtrate ran clear to ensure that the final pH of the sol solution was close to 4.0 (in order to form consistent final materials). To make TMOS and MTMS sols, 700 µL of water and 50 µL HCl (0.1 N) were added to 2.25 mL TMOS or MTMS and then sonicated for 20 min in ice-cold water. The 60% TMOS – 40% MTMS (v/v) mixture were prepared by proportionally dividing the 2.25 mL of silane to 1350 µL TMOS and 900 µL MTMS, mixing with water and acid and co-hydrolyzing in an ultrasonic bath, as described above. All prepared sols were stored on ice until use and used within one hour.

Monoliths for opacity screening were prepared by combining each of the sols with 2× PEG-doped assay buffer in a 1:1 (v/v) ratio, depositing 50 µL of the mixtures in a 96-well plate and allowing it to gel for 3 h prior to absorbance measurements at 400 nm using a

Tecan M1000 multimode plate reader. Poly(ethylene glycol) with various molecular weights ranging from 0.6 – 10 kDa, was used at five final concentrations from 0 – 10 % (w/v). Kinetic analysis of transmittance was done for the 60% TMOS – 40% MTMS (v/v) mixture with 0 – 10% (w/v) of 0.6 – 10 kDa PEG in a 96 well-plate by measuring absorbance at 400 nm every 5 min for 12 h.

Entrapment of Concatemeric Aptamer Complexes in Sol-Gel Derived Disks. Tripartite aptamer complexes (in a 1:1:6 Aptamer/FDNA/QDNA molar ratio) for entrapment were prepared at 2× final concentration in 2× PEG-doped assay buffer, heated at 90 °C for 5 min, cooled at room temperature and mixed in a 1:1 volume ratio with a freshly-prepared sol at room temperature. The aptamer-sol mixtures were deposited into the wells of a 96-well plate at a volume of 50 µL per well and allowed to gel and age for at least 3 h and then overlaid with assay buffer prior to washing and analysis.

The various sol-gel derived materials containing the reporter complexes were washed three times with 50 µL buffer at room temperature to remove any unencapsulated DNA from the material surface. Leaching of entrapped aptamers from the materials was determined by comparing the total fluorescence intensity prior to any washing to that of washed materials, as well as the fluorescence intensity of the combined wash solutions for all three washes. Fluorescence anisotropy of the wash solutions were also measured using the Tecan M1000 with excitation at 470 nm and emission at 520 nm (5 nm bandpasses) and was corrected for the instrumental G-factor. Following washing, materials were incubated at 25 °C for 10 min in the plate reader prior to target addition to the overlaid

buffer solution and fluorescence measurements. This experiment was also repeated with the monomeric versions of each aptamer, complexed in the same 1:1:6 ratio.

To test the sensitivity of the aptamer complexes in materials, following incubation and washing, ATP was added to the ATP-binding concatemer at final concentrations of 0 – 3 mM, while PDGF was added to the PDGF-binding concatemer at a final concentration range of 0 – 300 nM (2 μ L of each analyte solution was added at the appropriate concentration). The selectivity of entrapped concatemers to bind their specific target over structurally-related molecules was also assessed. The ATP-binding concatemer was incubated with ATP, CTP, GTP or UTP at a final concentration of 2 mM, while the concatemeric PDGF aptamer was incubated with PDGF, IGF-I, EGF and BSA at a final concentration of 200 nM.

To assess nuclease resistance upon entrapment, 1 U of DNase I was added directly to solution samples or the overlaying buffer of macroporous material samples containing either the ATP-binding or PDGF-binding concatemer complex. Degradation will cause liberation of FDNA and/or QDNA, resulting in a significant increase in fluorescence intensity. Degradation was thus assessed by measuring the time-dependent increases in fluorescence emission over a period of 60 min following addition of DNase I, and was compared to the emission changes for control samples without added DNase I.

Preparation of Monolithic Chromatography Columns. Both monomeric and concatemeric aptamers were entrapped in monolithic columns, where the original QDNA quencher moiety was replaced with a fluorescein (FAM)- or Cy5-labelled strand with an

identical sequence to produce F'DNA. The aptamers were combined with F'DNA in a 1:6 molar ratio at 2× final concentration in 2× PEG-doped assay buffer, heated at 90 °C for 5 min, and cooled at room temperature to anneal the F'DNA to the aptamer.

Monolithic columns were prepared by mixing the 60% TMOS – 40% MTMS (v/v) sol in a 1:1 volume ratio with the 2× PEG-doped assay buffer and immediately loading the mixture into 2 m of 250 µm i.d. fused-silica capillary. The final composition of the solution was 5% PEG (6 000 Da) containing either no DNA molecules, 600 nM F'DNA only, or 100 nM aptamer (concatemeric or monomeric aptamer) complexed with 600 nM F'DNA in 1× assay buffer. Columns were laid flat at room temperature in air for 3 h for gelation and preliminary aging to occur. Then, the ends of the capillaries were immersed in Eppendorf tubes containing 1× assay buffer and covered with Parafilm™ to prevent evaporation. The monoliths were further aged for at least 3 – 14 days at 4 °C. Columns were then cut into 10-cm pieces (discarding 10 cm segments from each end) and attached to an Eksigent 2D nanoLC pump with autosampler (Dublin, CA) using standard Upchurch Scientific fittings. Assay buffer was delivered to the column at a flow rate of 1 – 30 µL/min and compared to empty capillaries in order to measure backpressure and column robustness. For flow-through sensor assays, columns were first conditioned using 8 bed volumes of buffer to remove any free PEG. Assay buffer was introduced to the column at a flow rate of 1 µL/min and two 20 µL fractions were collected in Eppendorf tubes. Either ATP or PDGF in buffer (at final concentrations of 0 – 3 mM for ATP or 0 – 300 nM for PDGF), human serum with or without 200 nM PDGF, or a mixed solution of 2 mM ATP and 200 nM PDGF in buffer was then added to the column using the

autosampler and a third 20 mL fraction was collected. Buffer was then re-introduced into the column and a final fourth fraction of 20 mL volume was collected.

Fluorescence Intensity and Anisotropy Measurements. All fluorescence measurements were performed using a Tecan Infinite[®] M1000 platereader in fluorescence mode. Excitation was done at 490 nm (5-nm bandpass) and emission was measured at 520 nm (5-nm bandpass) with a 20 μ s integration time using the bottom-read setting. Kinetic measurements in solution and monolithic disks were performed to assess signal response upon addition of a given target (or DNase I) using fluorescence intensity reads every 1 min for both baseline (before target/DNase addition; 10 min) and assay (after addition of target/DNase; 1 h) measurements, with orbital shaking of 2.5 mm amplitude for 5 s between each measurement to ensure proper mixing. Raw fluorescence intensity measurements were normalized to F/F_0 where F is the endpoint fluorescence intensity and F_0 is the initial fluorescence intensity prior to QDNA/target addition. Fluorescence scans of collected column fractions were performed using an excitation wavelength of 490 nm (5-nm bandpass) and measuring emission from 500 – 560 nm (5 nm bandpass) for fluorescein or an excitation wavelength of 645 nm (5 nm bandpass) and measuring emission from 655 – 715 nm (5-nm bandpass) for Cy5, using bottom-read mode. Fluorescence anisotropy measurements were performed using a 470 nm excitation wavelength and 520 nm emission wavelength (5 nm bandpass) in top-read mode. All assays were carried out in triplicate with background fluorescence subtraction at 25 °C.

DLS Measurements. DNA sizing was performed using a Malvern Instruments Zetasizer Nano ZS to measure light scattering intensity. Samples were placed in a plastic cuvette and three separate samples of each DNA construct at 1 μM were measured using 10 runs in automatic mode at 20 °C.

SEM Imaging. Samples for SEM imaging were aged in air for at least 5 days at room temperature before being cut to expose a fresh surface for mounting. Scanning electron microscopy imaging was performed using a FEI Magellan XHR 400 at 1 kV. Energy dispersive x-ray spectroscopy was performed using the same scanning electron microscope with a 5 keV beam.

2.6 Acknowledgements

The authors thank the Natural Sciences and Engineering Research Council of Canada for financial support for this work. The EM research described in this paper was performed at the Canadian Centre for Electron Microscopy at McMaster University, which is supported by NSERC and other government agencies. Y.L. holds the Canada Research Chair in Directed Evolution of Nucleic Acids. J.D.B. holds the Canada Research Chair in Bioanalytical Chemistry and Biointerfaces.

2.7 References

- (1) Avnir, D.; Braun, S.; Lev, O.; Ottolenghi, M. *Chem. Mater.* **1994**, *6*, 1605–1614.
- (2) Bhatia, R. B.; Brinker, C. J.; Gupta, A. K.; Singh, A. K. *Chem. Mater.* **2000**, *12*, 2434–2441.
- (3) Kandimalla, V.; Tripathi, V. S.; Ju, H. *Crit. Rev. Anal. Chem.* **2006**, *36*, 73–106.
- (4) Avnir, D.; Coradin, T.; Lev, O.; Livage, J. *J. Mater. Chem.* **2006**, *16*, 1013–1030.
- (5) Brennan, J. D. *Acc. Chem. Res.* **2007**, *40*, 827–835.
- (6) Monton, M. R. N.; Forsberg, E. M.; Brennan, J. D. *Chem. Mater.* **2012**, *24*, 796–811.
- (7) Forsberg, E. M.; Sicard, C.; Brennan, J. D. *Annu. Rev. Anal. Chem.* **2014**, *7*, 337–359.
- (8) Cruz-Aguado, J. A.; Chen, Y.; Zhang, Z.; Brook, M. A.; Brennan, J. D. *Anal. Chem.* **2004**, *76*, 4182–4188.
- (9) Hodgson, R. J.; Chen, Y.; Zhang, Z.; Tleugabulova, D.; Long, H.; Zhao, X.; Organ, M.; Brook, M. A.; Brennan, J. D. *Anal. Chem.* **2004**, *76*, 2780–2790.
- (10) Rupcich, N.; Nutiu, R.; Li, Y.; Brennan, J. D. *Anal. Chem.* **2005**, *77*, 4771–4778.
- (11) Besanger, T. R.; Hodgson, R. J.; Guillon, D.; Brennan, J. D. *Anal. Chim. Acta* **2006**, *561*, 107–118.
- (12) Besanger, T. R.; Hodgson, R. J.; Green, J. R. A.; Brennan, J. D. *Anal. Chim. Acta* **2006**, *564*, 106–115.
- (13) Shen, Y.; Mackey, G.; Rupcich, N.; Gloster, D.; Chiuman, W.; Li, Y.; Brennan, J. D. *Anal. Chem.* **2007**, *79*, 3494–3503.

- (14) Forsberg, E. M.; Green, J. R. A.; Brennan, J. D. *Anal. Chem.* **2011**, *83*, 5230–5236.
- (15) Carrasquilla, C.; Lau, P. S.; Li, Y.; Brennan, J. D. *J. Am. Chem. Soc.* **2012**, *134*, 10998–11005.
- (16) Zhao, Q.; Li, X. F.; Le, X. C. *Anal. Chem.* **2008**, *80*, 3915–3920.
- (17) Zhao, Q.; Li, X. F.; Shao, Y.; Le, X. C. *Anal. Chem.* **2008**, *80*, 7586–7593.
- (18) Deng, N.; Liang, Z.; Liang, Y.; Sui, Z.; Zhang, L.; Wu, Q.; Yang, K.; Zhang, L.; Zhang, Y. *Anal. Chem.* **2012**, *84*, 10186–10190.
- (19) Forsberg, E. M.; Brennan, J. D. *Anal. Chem.* **2014**, *86*, 8457–8465.
- (20) Wang, Z.; Zhao, J. C.; Lian, H. Z.; Chen, H. Y. *Talanta* **2015**, *138*, 52–58.
- (21) Fire, A.; Xu, S. Q. *Proc. Natl. Acad. Sci.* **1995**, *92*, 4641–4645.
- (22) Liu, D.; Daubendiek, S. L.; Zillman, M. A.; Ryan, K.; Kool, E. T. *J. Am. Chem. Soc.* **1996**, *118*, 1587–1594.
- (23) Vlček, Č.; Pačes, V. *Gene* **1986**, *46*, 215–225.
- (24) Blanco, L.; Bernad, A.; Lázaro, J. M.; Martín, G.; Garmendia, C.; Salas, M.; Bernads, A.; Lharo, J. M.; Martins, G. *J. Biol. Chem.* **1989**, *264*, 8935–8940.
- (25) Zhu, G.; Hu, R.; Zhao, Z.; Chen, Z.; Zhang, X.; Tan, W. *J. Am. Chem.* **2013**, *135*, 1–10.
- (26) Hu, R.; Zhang, X.; Zhao, Z.; Zhu, G.; Chen, T.; Fu, T.; Tan, W. *Angew. Chemie - Int. Ed.* **2014**, *53*, 5821–5826.
- (27) Carrasquilla, C.; Little, J. R. L.; Li, Y.; Brennan, J. D. *Chem. Eur. J.* **2015**, *21*, 7369–7373.
- (28) Smith, A. M. E.; Fortuna, J.; Forsberg, E. M.; Brennan, J. D. *RSC Adv.* **2014**, *4*,

15952–15960.

- (29) Carrasquilla, C.; Brennan, J. D. *Methods* **2013**, *63*, 255–265.
- (30) Huizenga, D. E.; Szostak, J. W. *Biochemistry* **1995**, *34*, 656–665.
- (31) Green, L. S.; Jellinek, D.; Jenison, R.; Östman, A.; Heldin, C. H.; Janjic, N. *Biochemistry* **1996**, *35*, 14413–14424.
- (32) Nutiu, R.; Li, Y. *J. Am. Chem. Soc.* **2003**, *125*, 4771–4778.
- (33) Nutiu, R.; Li, Y. *Chem. - A Eur. J.* **2004**, *10*, 1868–1876.
- (34) Nutiu, R.; Li, Y. *Methods* **2005**, *37*, 16–25.
- (35) Del Vecchio, P.; Esposito, D.; Ricchi, L.; Barone, G. *Int. J. Biol. Macromol.* **1999**, *24*, 361–369.
- (36) Bonner, G.; Klibanov, a M. *Biotechnol. Bioeng.* **2000**, *68*, 339–344.
- (37) Hui, C. Y.; Li, Y.; Brennan, J. D. *Chem. Mater.* **2014**, *26*, 1896–1904.
- (38) Schriemer, D. C.; Bundle, D. R.; Li, L.; Hindsgaul, O. *Angew. Chem., Int. Ed.* **1999**, *37*, 3383–3387.
- (39) Peyrin, E. *J. Sep. Sci.* **2009**, *32*, 1531–1536.
- (40) Pichon, V.; Brothier, F.; Combès, A. *Anal. Bioanal. Chem.* **2015**, *407*, 681–698.
- (41) Du, F.; Guo, L.; Qin, Q.; Zheng, X.; Ruan, G.; Li, J.; Li, G. *TrAC - Trends Anal. Chem.* **2015**, *67*, 134–146.

2.8 Appendix

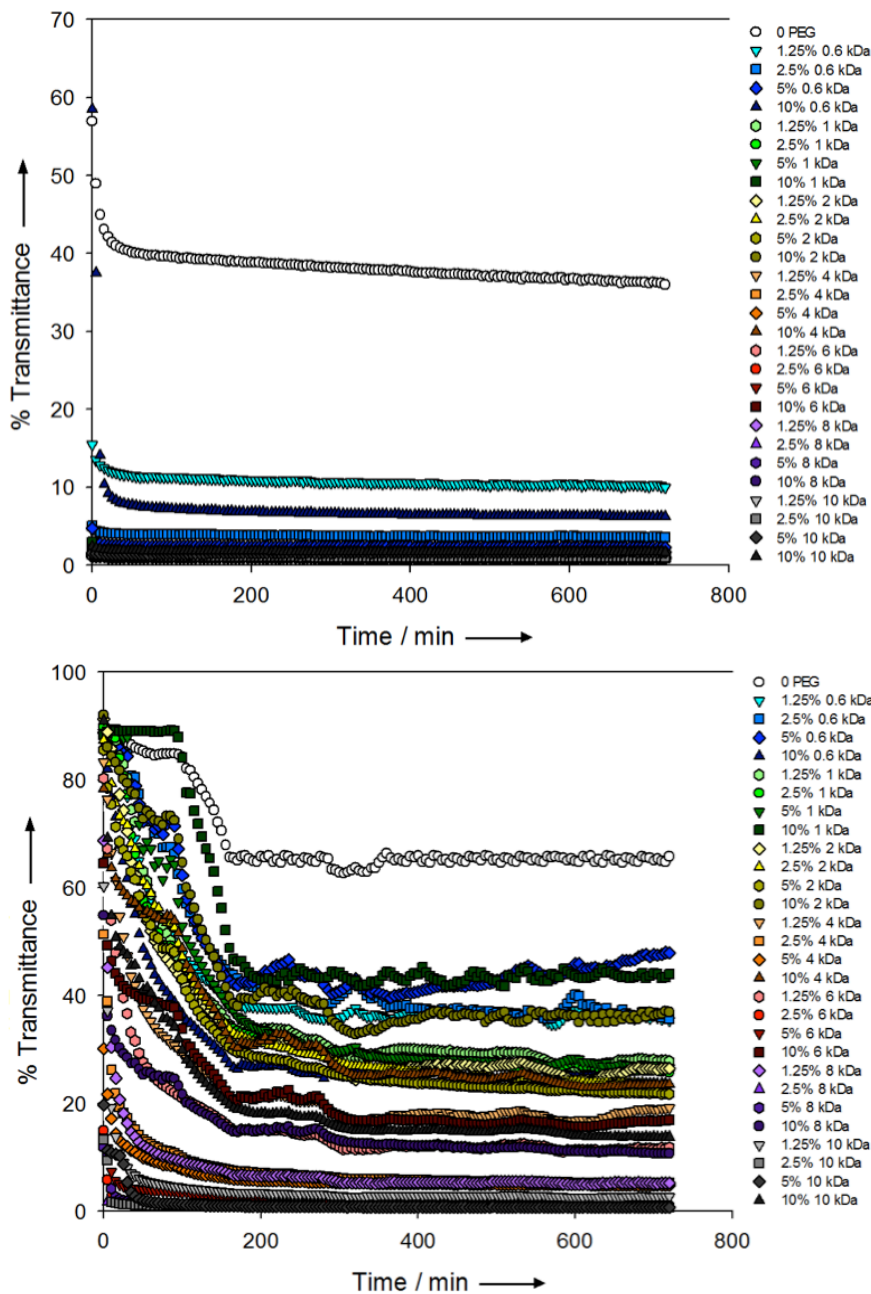


Figure S2.1. Time-resolved changes in transmittance of sol-gel derived materials. Transmittance at 400 nm of SS (top) and 40% MTMS (bottom) mixed in assay buffer with 0 – 10 kDa PEG at various concentrations over 12 h as samples undergo phase separation and evolve over time.

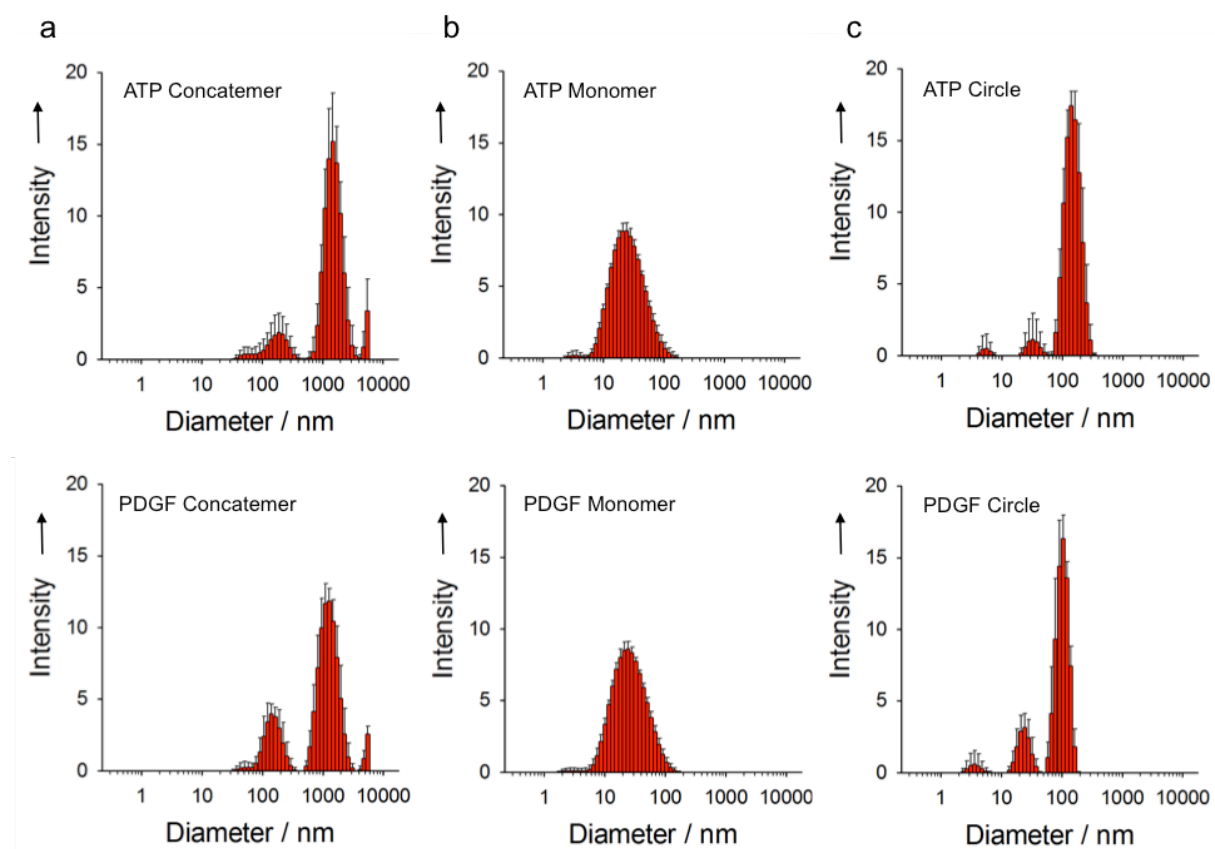


Figure S2.2. DLS measurements of DNA constructs in solution. Hydrodynamic size distributions of a) concatemeric, b) monomeric and c) circular template constructs for the ATP aptamer (top) and PDGF aptamer (bottom) in solution as measured by dynamic light scattering intensity.

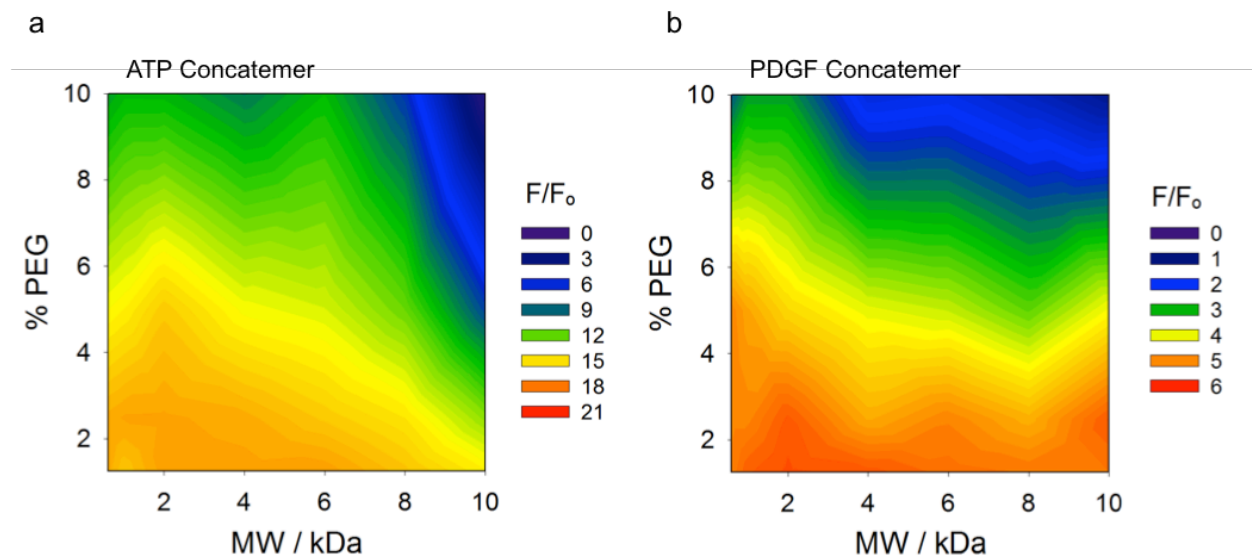


Figure S2.3. Signal enhancement of concatemeric reporters in PEG-doped buffer. Fluorescence signal response of the a) concatemeric ATP aptamer with 2 mM ATP and b) concatemeric PDGF aptamer with 200 nM PDGF, in solution containing increasing concentrations of 1.25 – 10 kDa PEG.

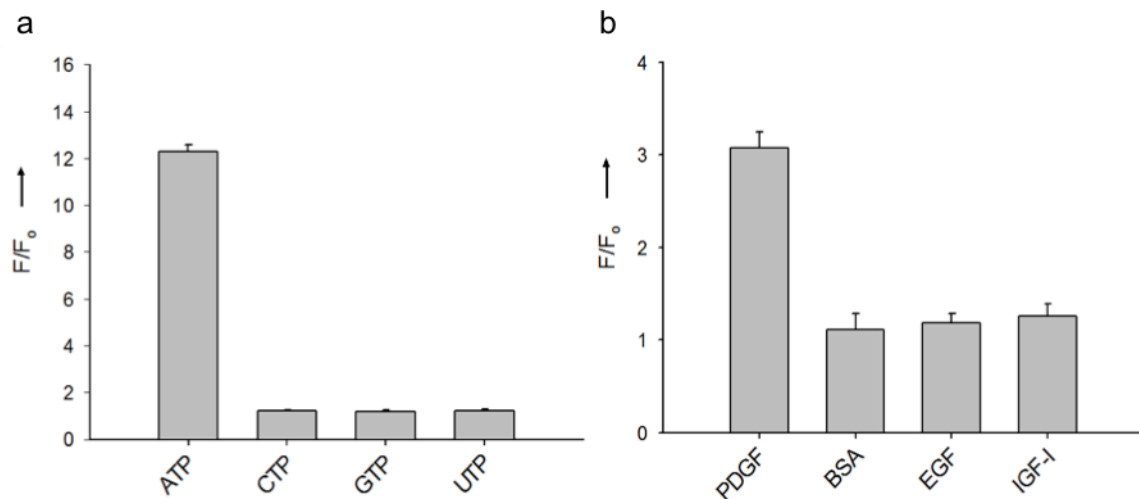


Figure S2.4. Selectivity of entrapped concatemeric aptamers. Selectivity of the a) concatemeric ATP aptamer to different nucleotides at 2 mM concentration and b) concatemeric PDGF aptamer to different growth factors and proteins at 200 nM concentration, entrapped in Macro 40% MTMS.

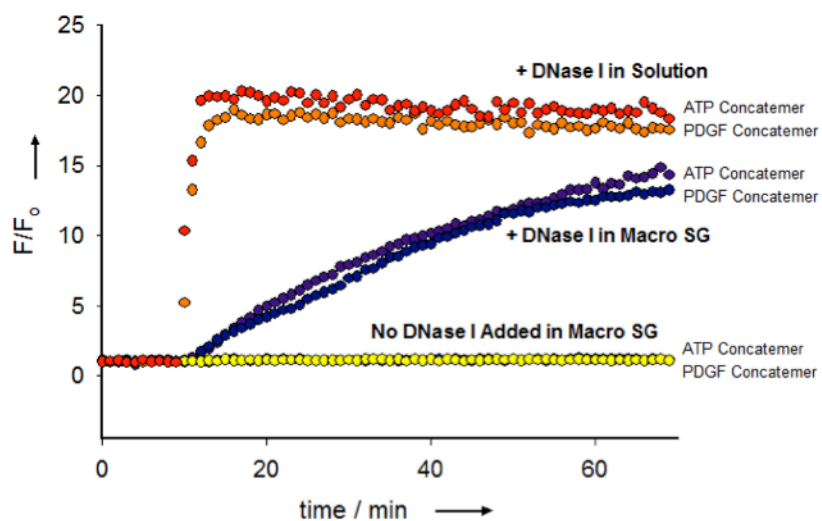


Figure S2.5. Concatemeric aptamer emission intensity upon exposure to DNase I. Fluorescence measurements over time (1 hr) after addition of 1 unit of DNase I to the ATP-binding and PDGF-binding concatemeric aptamer reporters in solution or entrapped within the Macro 40% MTMS material.

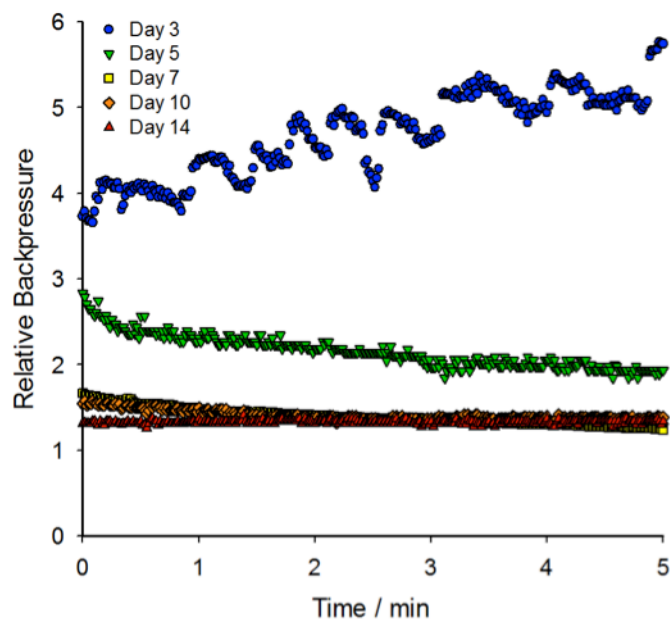


Figure S2.6. Backpressure of monolithic columns upon aging. Backpressure of monolithic columns relative to empty capillaries (indicated by a relative backpressure of 1 at ~15 PSI) after various aging periods at a flow rate of 1 $\mu\text{L}/\text{min}$. Columns were used for target detection assays only after at least 7 days of aging.

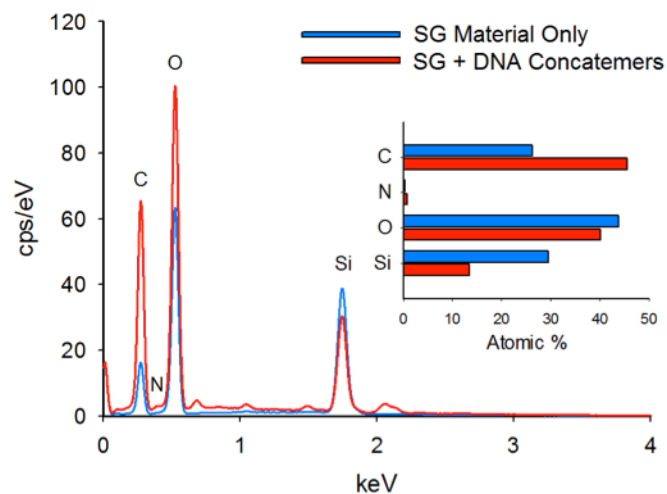


Figure S2.7. EDX analysis of sol-gel derived monolithic columns. A spectral overlay comparing the differences in elemental composition between a monolithic column with versus without entrapped concatemeric aptamers. Inset: the relative atomic contribution from C, N, O and Si for a sol-gel derived monolithic column with or without entrapped concatemeric aptamer amplicons.

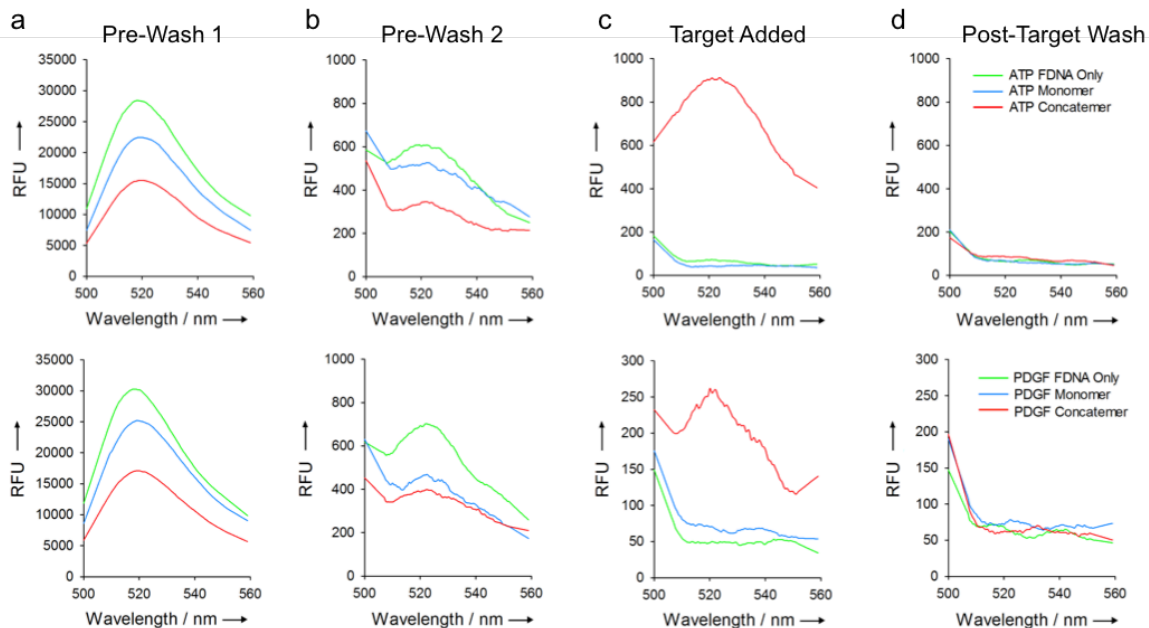


Figure S2.8. Fluorescence Scans of Column Fractions. Emission scans of eluate from monolithic columns containing various entrapped DNA molecules, divided into four fractions: a) pre-wash 1, b) pre-wash 2, c) elution with target and d) post-target wash. Fractions 1, 2 and 4 serve as wash steps with buffer only and fractions 3 contains either 2 mM ATP (top) or 200 nM PDGF (bottom) for the appropriate column.

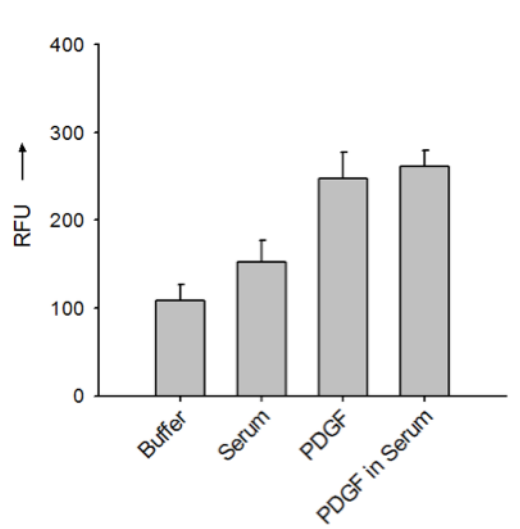


Figure S2.9. Column response to PDGF in a complex sample. PDGF concatemer-doped monolithic column response to 0 or 200 nM PDGF in either buffer or undiluted human serum.

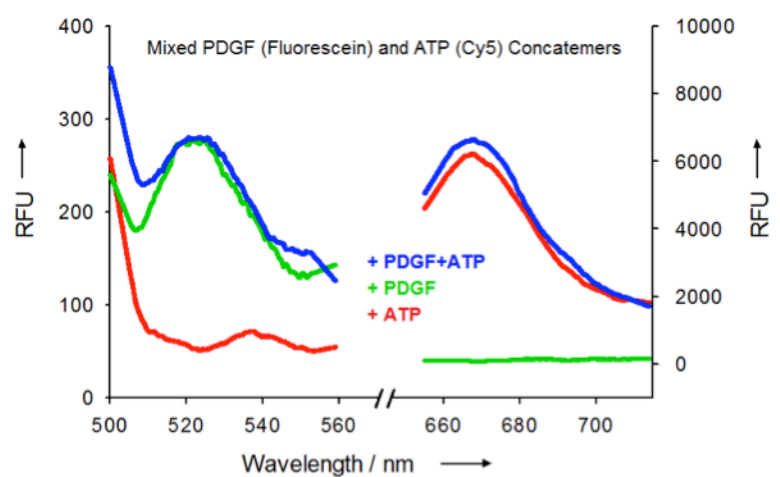


Figure S2.10. Response of mixed concatemer columns. Columns containing both PDGF-FAM and ATP-Cy5 concatemers were exposed to either 2 mM ATP (red line), 200 nM PDGF (green line) or a mixture of 200 nM PDGF and 2 mM ATP in buffer (blue line). Left spectra show emission of FAM originating from the PDGF aptamer, right spectra show emission of Cy5 originating from the ATP aptamer.

Table S2.1. DNA oligonucleotide sequences for aptamer reporter systems.

DNA oligonucleotide	Sequence (5'→3')
Linear ATP Aptamer Circular Template	TGTCT TCGCC TATAG TGAAC CTTCC TCCGC AATAC TCCCC CAGGT ATCTT TCGAC TAAGC ACC
ATP Aptamer Ligation Template	GGCGA AGACA GGTGC TTAGT C
ATP Aptamer Primer	GGGGG AGTAT TGCGG AGGAA
Linear PDGF Aptamer Circular Template	TGCAG CGACT CACAG GATCA TGGTG ATGCT CTACG TGCCG TAGCC TGCCC TTTCG ACTAC C
PDGF Aptamer Ligation Template	GAGTC GCTGC AGGTA GTCGA A
PDGF Aptamer Primer	CGTAG AGCAT CACCA TGATC
ATP aptamer FDNA (ATP-FDNA)	(fluorescein)CGACT AAGCA CCTGT C
ATP aptamer QDNA (ATP-QDNA/FDNA/F'DNA)	CCCAG GTATC TT(dabcyl/fluorescein/Cy5)
ATP aptamer monomeric construct (ATP-Apt)	TCACT ATAGG CGAAG ACAGG TGCTT AGTCG AAAGA TACCT GGGGG AGTAT TGCGG AGGAA GGT
PDGF aptamer FDNA (PDGF-FDNA)	(fluorescein)GACTA CCTGC AGCGA
PDGF aptamer QDNA (PDGF-QDNA/FDNA/F'DNA)	AGCCT GCCCT TT(dabcyl/fluorescein/fluorescein)
PDGF aptamer monomeric construct (PDGF-Apt)	TGAGT CGCTG CAGGT AGTCG AAAGG GCAGG CTACG GCACG TAGAG CATCA CCATG ATCCT G

Table S2.2. Composition of the 24 macroporous sol-gel derived materials chosen for aptamer entrapment.

Precursor	PEG MW (kDa)	[PEG] (%)
SS	0.6	1.25
SS	0.6	2.5
SS	0.6	5
SS	1	1.25
SS	1	2.5
SS	1	5
TMOS	4	1.25
TMOS	4	2.5
TMOS	4	5
TMOS	6	1.25
TMOS	6	2.5
TMOS	6	5
TMOS	8	1.25
TMOS	8	2.5
TMOS	8	5
40% MTMS	4	1.25
40% MTMS	4	2.5
40% MTMS	4	5
40% MTMS	6	1.25
40% MTMS	6	2.5
40% MTMS	6	5
40% MTMS	8	1.25
40% MTMS	8	2.5
40% MTMS	8	5

Table S2.3. Fluorescence polarization from ATP or PDGF concatemer, monomer and FDNA in solution or leached from materials.

	Solution (mP)	Leached (mP)
ATP Concatemer	110 ± 2	70 ± 4
ATP Monomer	105 ± 1	107 ± 6
ATP FDNA only	61 ± 2	66 ± 3
PDGF Concatemer	122 ± 1	81 ± 9
PDGF Monomer	111 ± 1	116 ± 7
PDGF FDNA only	69 ± 1	76 ± 4

CHAPTER 3 | EVALUATION OF DNAZYME-BASED NANOFLOWERS FOR BACTERIAL DETECTION

The author designed the circle and performed all of the reactions that led to the fabrication of the EC1 DNAzyme-based nanoflowers. In addition, the author completed all of the other experiments and data analysis, including solution assays and electron microscope imaging. The preliminary draft of this chapter was completed by the author and Dr. John Brennan.

3.1 Abstract

Rolling circle amplification (RCA) has been used for elongating a variety of DNA species into concatenated superstructures. Among such species, a number of DNA aptamers have been concatenated to allow amplification of biosensing signals or as a platform for DNA immobilization. While concatenated aptamers have been described, there is currently no studies reporting the formation of concatenated DNAzymes. Herein, RCA has been used to produce a concatenated EC1 DNAzyme for *Escherichia coli* detection. The concatenated DNAzymes were salt aged into DNA nanoflower superstructures that are megadalton in size, as these superstructures were evaluated in terms of performance for deection of *E. coli* bacteria. Preliminary studies demonstrated that the concatenated DNAzyme was able to produce a fluorescence signal upon introduction of *E. coli* intracellular matrix (CIM). The nanoflower superstructures cleaved the fluorogenic substrate in the presence of target more effectively than the monomer DNAzyme when used at a lower concentration.

3.2 Introduction

Functional nucleic acids (FNAs), including DNA/RNA aptamers and DNAzymes, are efficient recognition elements for the detection of small molecules,¹⁻⁵ proteins,⁶ and cells.⁷⁻⁹ The detection of the target can be performed using the FNA in monomeric or concatemeric form, depending on the application. For instance, concatemeric FNAs can be used for signal amplification,¹⁰⁻¹² or as biosensors while entrapped within materials.¹³ Concatemers are large single-stranded DNA oligomers containing tandem repeat units of the monomer sequence, and are produced through rolling circle amplification (RCA). RCA is a simple process that extends a short primer annealed to a circle template to produce a long single-stranded DNA oligomer that contains tandem repeat units of the complementary sequence to the circle.^{11,14-17} Concatemeric DNA strands produced by RCA can reach sizes in the megadalton range, which can allow immobilization of the biomolecules with platforms, such as paper-based devices or capillary columns, without requiring covalent or affinity-based interactions.^{6,13} Aptamers have been shown to remain active in the concatenated form, however there have been limited reports of using concatemeric DNAzymes in biosensing applications.¹⁸

DNAzymes are catalytically active DNA oligomers that cleave a substrate consisting of a specific DNA or RNA sequence, while in the presence of target.¹ There are either DNA-cleaving or RNA-cleaving DNAzymes, which are designed using *in vitro* selection.^{7,19,20} A RNA-cleaving DNAzyme is selected for based on successful cleavage of a chimeric substrate that is composed of a DNA sequence containing a ribonucleotide in the middle of the DNA strand.¹⁹ RNA-cleaving DNAzymes should not be capable of

cleaving substrates containing exclusively deoxyribonucleotides however, since ribonucleotides are 100,000 times more susceptible to hydrolytic cleavage than deoxyribonucleotides.¹ Additionally, the substrate can be covalently-linked to the catalytically active DNAzyme strand in the *cis*-conformation, or the substrate can be a separate strand hybridized to the DNAzyme in the *trans*-conformation. DNAzymes in the *cis*-conformation are more active than *trans*-DNAzymes, likely because the substrate is covalently-linked in close proximity to the catalytic site and does not have to rely on hydrogen bonds to remain hybridized to the catalytic strand.²¹

There are fewer examples of concatenated DNAzymes used in biosensing assays than aptamers,¹¹ likely due to the stringent environmental conditions required for DNAzyme activity.¹ DNAzymes require divalent metal ions, specific buffer composition, pH, and temperature to fold into the catalytically active conformation. The DNAzyme must be folded into the proper structure for activity upon target addition, meanwhile aptamers tend to be more flexible and do not require a specific, rigid structure to structure-switch.²² These structural requirements make DNAzymes less amenable to concatenation into active DNAzyme units.

As an initial step toward the use of concatenated DNAzymes in biosensing applications, we investigated the properties of the concatenated EC1 DNAzyme in solution. The EC1 DNAzyme was chosen for investigation because the identity of the protein target within the crude intracellular matrix (CIM) of *Escherichia coli* is unknown, and future entrapment within affinity chromatography columns may be of use for target extraction.

The RNA-cleaving EC1 DNAzyme is used for *E. coli* detection in bioassays by cleaving a substrate (FS28) containing a ribonucleotide flanked by two deoxyribonucleotides (one labelled with fluorescein and the other labelled with a dabcy1 quencher). Once the DNAzyme structure has folded in the proper conformation and hybridized to the substrate efficiently, the DNAzyme can bind to the target located within the CIM of *E. coli* and cleave the ribonucleotide contained in the FS28 substrate to produce fluorescence. The fluorescence is produced by the release of the quencher segment of the substrate upon catalytic cleavage by the DNAzyme.

Herein, we demonstrate the design of the concatenated EC1 DNAzyme and preliminary activity studies in solution. The *trans*-DNAzyme was used for concatenation because it is impossible to replicate the covalently-linked fluorogenic substrate (*cis*-DNAzyme) using RCA. The FS28 substrate was annealed to the DNAzymes following concatenation. Additionally, the concatenated DNAzymes were salt aged into nanoflower superstructures,^{23,24} to determine if such 3D superstructures provided enhanced activity or signalling relative to native 2D RCA products.

3.3 Experimental Section

3.3.1 Materials. The chimeric DNA/RNA oligonucleotide substrate (FS28) was synthesized and deprotected by W. M. Keck Oligonucleotide Synthesis Facilities (Yale University, New Haven, CT, USA), and purified by 10% denaturing polyacrylamide gel electrophoresis (dPAGE). All other standard DNA oligonucleotides were synthesized and purified using high-performance liquid chromatography (HPLC) by Integrated DNA

Technologies (Coralville, IA). T4 polynucleotide kinase (PNK; with 10× PNK reaction buffer), T4 ligase (with 10× DNA ligase buffer), polyethylene glycol (PEG; 4,000 Da) 10 mM dNTPs, phi29 DNA polymerase (with 10× phi29 DNA polymerase buffer), ATP solution (100 mM), FastDigest HpaII, GeneRuler™ 1 kb Plus DNA ladder and 10,000× SYBR Gold DNA stain were purchased from ThermoFisher Scientific (Ottawa, ON). *E. coli* K12 (MG1655) and *B. subtilis* are regularly maintained in our laboratory. A Millipore Milli-Q Synthesis A10 water purification system was used to purify water prior to use.

3.3.2 Methods

Preparation of Concatemeric (2D) and Nanoflower (3D) DNA Amplicons. The concatemeric amplicons were prepared using the sequences listed in Table S3.1 as described elsewhere and briefly below.⁶ Firstly, a total of 300 pmol of anti-EC1 linear circular template was phosphorylated at the 5'-end using T4 PNK at 37 °C for 30 min in a solution of 2 mM ATP and 1× PNK reaction buffer. The PNK was deactivated by heating at 90 °C for 5 min, and the solution was cooled to room temperature. The resultant phosphorylated DNA was circularized by performing ligation with 10 U of T4 ligase at room temperature for 1 h in a solution of 400 pmol of EC1 template primer, 5 % PEG (4,000 Da), and 1× ligase buffer. The ligase was deactivated by heating at 65 °C for 10 min and the solution was cooled to room temperature prior to performing ethanol precipitation. The circularized templates were purified using 10 % dPAGE (Figure S3.1), followed by ethanol precipitation and resuspension in water.

The RCA reaction to produce concatemeric EC1 DNAzyme was performed by mixing 1 pmol of circular template with 2.25 pmol of primer and 5 μ L of 10 \times phi29 polymerase buffer. The solution was heated at 90 $^{\circ}$ C for 1 min and cooled to room temperature prior to adding 5 μ L of 10 mM dNTPs and 10 U of phi29 DNA polymerase (50 μ L total volume). The mixture was incubated for 45 min at 30 $^{\circ}$ C, followed by enzyme deactivation at 65 $^{\circ}$ C for 10 min. The resultant products were the 2D DNA concatemers. The 3D DNA constructs were fabricated by salt aging the 2D DNA oligomers in the polymerase buffer for 12 h prior to purification by centrifugation using a 100 kDa Nanosep[®] spin column. The resultant DNA samples were analyzed on a 0.6 % agarose gel in comparison to samples that did not contain polymerase and only circle (Figure S3.2). The DNA constructs were quantified using a TECAN Infinite[®] M1000 plate reader (absorbance at 260 nm). The approximate molar concentration was calculated based on one repeat of the monomer sequence since the exact size of the RCA product was unknown.

Successful concatemer production was confirmed by restriction enzyme digestion with FastDigest HpaII. Double-stranded DNA was required for digestion, so the sequence compH was first annealed to the concatemers by heating 20 pmol of the concatemer and 300 pmol of compH to 90 $^{\circ}$ C for 1 min, followed by cooling to room temperature. Then, 2 μ L of FastDigest HpaII was added along with 1 μ L of 10 \times FastDigest green buffer (for a total volume of 10 μ L). The solution was incubated at 37 $^{\circ}$ C for 24 h. The restriction enzyme was deactivated by heating at 65 $^{\circ}$ C for 5 min. A 10 % dPAGE gel confirmed that digestion was successful (Figure S3.3).

Preparation of Crude Intracellular Matrix (CIM). The *E. coli* K12 and *B. subtilis* CIM were prepared as previously reported and briefly below.¹⁷ A 2 mL Luria broth (LB) culture was inoculated with *E. coli* K12 cells from a glycerol stock and incubated at 37 °C and 250 rpm for 6 h. The cells were divided into 1 mL fractions and centrifuged at 13,000 xg for 10 min. The cells were resuspended in 200 µL of 1× reaction buffer (50 mM HEPES, 150 mM NaCl, 15 mM MgCl₂, pH 7.5) (5× concentration factor since 1 mL was resuspended in 200 µL). The cells were frozen until CIM was needed. *B. subtilis* was prepared in the same manner, however a single colony from a previously grown LB plate was used for inoculation.

The frozen cells were thawed and sonicated for 1 min, followed by incubation on ice for 5 min. The sonication/incubation cycle was repeated three times. The cell debris was centrifuged at 13,000 xg for 10 min and the supernatant was removed as the CIM. In some cases, the 200 µL of CIM was fractionated using a 30 kDa Amicon[®] Ultra Millipore spin column by centrifuging at 10,000 xg for 10 min. The concentrate was collected by inverting the filter in a new tube and centrifuged at 1,000 xg for 3 min. The volume was increased to 200 µL with 1× reaction buffer.

Kinetic Fluorescence Intensity Measurements in Solution. The TECAN Infinite[®] M1000 plate reader was used to perform all fluorescence measurements. The measurements were performed in bottom-read mode with an excitation wavelength of 488 nm (5-nm bandpass) and emission wavelength set to 520 nm (5-nm bandpass) with a 20 µs integration time. The fluorescence response of the monomer, 2D and 3D DNA

concatemers to target were compared in solution using Greiner half-area 96-well plates. The FS28 concentration remained constant in all experiments at 50 nM, meanwhile the DNA construct was varied to determine the ideal concentration. Generally, 1 μ M DNA construct concentration was used in the assays, which was hybridized to the FS28 substrate prior to performing the assay. The DNA construct and FS28 were hybridized by heating the strands in 1 \times reaction buffer at 90 °C for 1 min, followed by cooling to room temperature. The baseline fluorescence intensity was measured every 1 min for 5 min and then 12.5 μ L of CIM was added to the wells for a final CIM concentration of 25 % (v/v) with a total volume of 50 μ L per well. The fluorescence intensity measurements continued every 1 min for an additional 60 min. The background was accounted for by subtracting the fluorescence of the EC1M construct from each of the EC1 constructs at each measured time point. The background adjusted fluorescence intensity measurements were normalized to F/F_0 by dividing each fluorescence measurement by the initial fluorescence intensity (F_0) after CIM addition. All assays were performed in triplicate at 25 °C.

SEM Imaging. The 3D DNA nanoflowers were solvent evaporated at room temperature on nitrocellulose prior to the addition of a 5 nm gold coating. A JEOL JSM-7000F scanning electron microscope was used to perform the nanoflower imaging with an electron beam set at 3 kV.

TEM Imaging. The 3D DNA nanoflowers were prepared by solvent evaporation on a carbon grid for TEM imaging, which was performed using a JEOL 2010F transmission electron microscope.

3.4 Results and Discussion

EC1 Nanoflower Production: The anti-EC1 circle was designed to encode the complementary sequence to the monomer EC1 sequence (*trans*-conformation) that was the most active in previous assays.²¹ The monomer was 71 base pairs in length and the circle was designed with an additional 14 nucleotides to act as a spacer to allow the RCA product units to fold in the proper conformation. The “mfold” web server for computational molecular biology was used to predict the conformation of the long-chain DNA strands and ensure the majority of the repetitive units folded in the same manner as the EC1 monomer. The circle was successfully ligated (Figure S3.1) and the RCA reaction produced long-chain DNA strands (Figure S3.2). Successful RCA resulted in smearing within the agarose gel due to the various strand lengths that are produced from the polymerase releasing the amplified strand at different times. In addition, the large size of the products generally caused most of the product to remain in the wells or barely enter the pores of the gel. Restriction enzyme digestion of the amplified product further confirmed the production of long-chain DNA strands (Figure S3.3). There were several bands in the digested sample, which indicated DNA strands were cleaved into different sizes.

The salt aging process of the 2D concatemers resulted in the production of 3D nanoflowers ranging in size from $\sim 0.3 \mu\text{m}$ to $1.6 \mu\text{m}$. Both the TEM images (Figure 3.1) and SEM images (Figure 3.2A and 3.2B) revealed the petal-like morphology that the DNA superstructures form upon salt aging. The 2D concatemers were too small for SEM imaging, which further indicated the role that salt aging has in folding the DNA into large superstructures. The salt aging allowed the long-chain concatemers to aggregate together to form these large superstructures.²³ The nanoflowers were resistant to degradation when *E. coli* CIM was added (Figure 3.2C and 3.2D). Most of the nanoflowers seemed to be joined by a dense polymer network, however that is likely due to the solvent evaporation of the CIM. Interestingly, the nanoflowers appeared to have degraded slightly after incubation in CIM, as the characteristic petal-like structure was less distinguishable. This may suggest that there are nucleases present in the CIM that are able to slowly digest even the 3D DNA superstructures, though the rate of degradation appears to be slow.

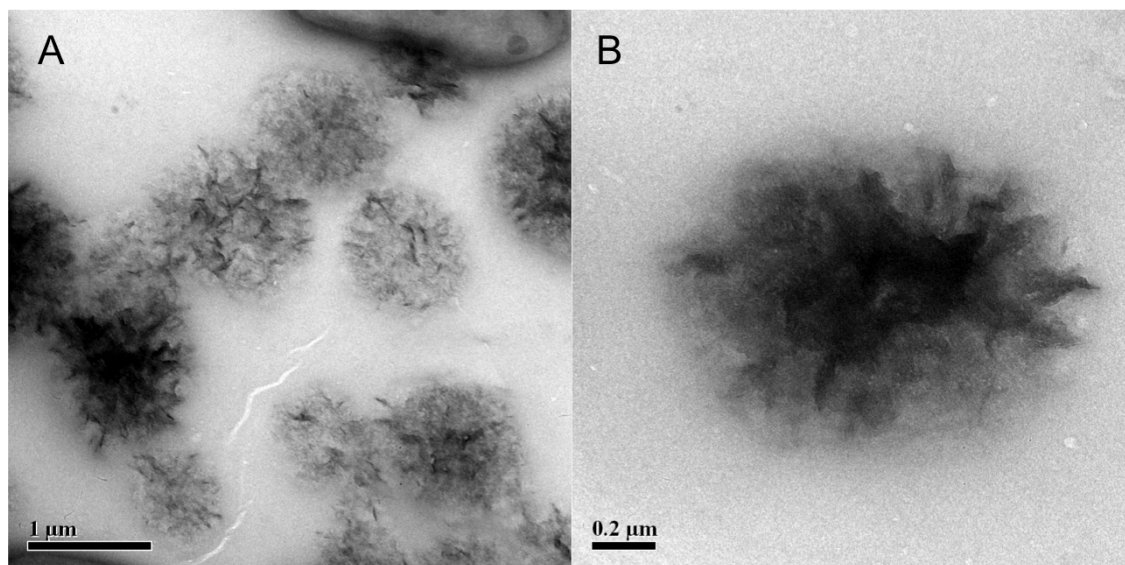


Figure 3.1. TEM images of the DNA nanoflowers.

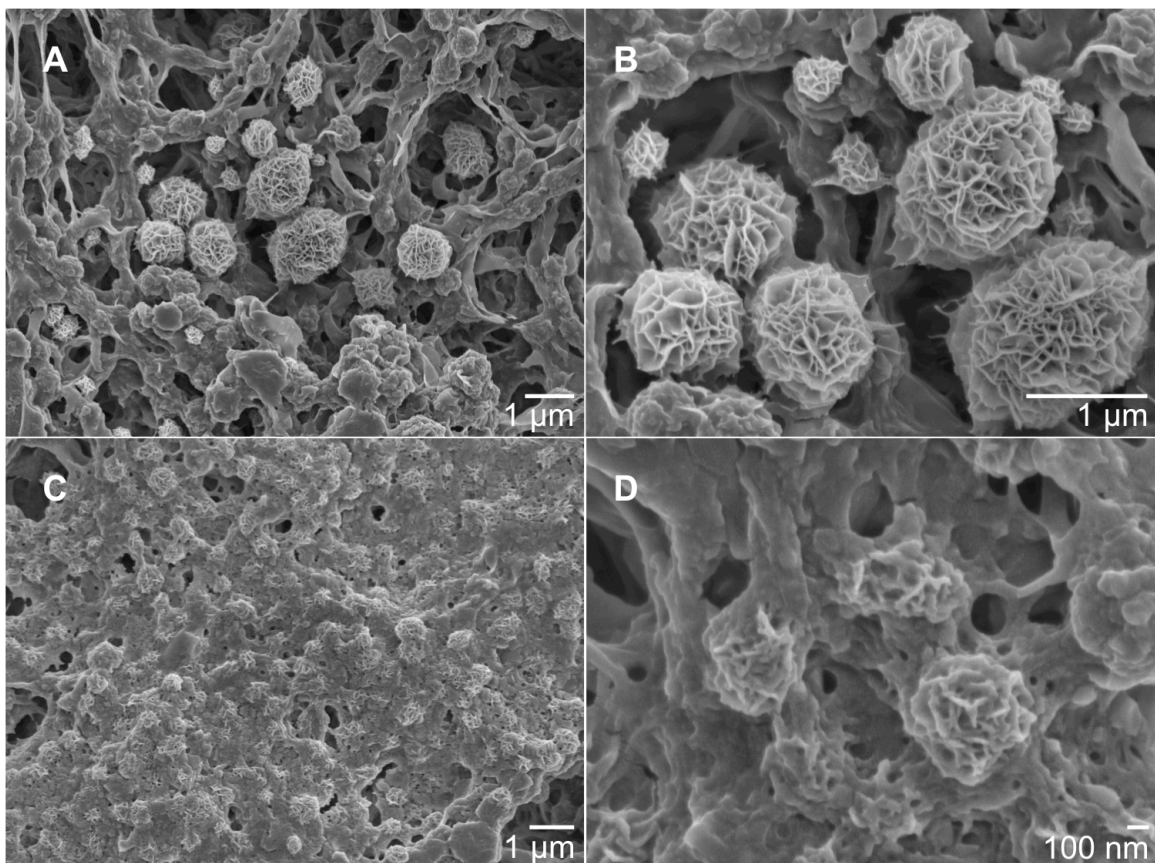


Figure 3.2. SEM images of the DNA nanoflowers in (A,B) solution and (C,D) after incubation in *E. coli* CIM for 1 hour. The solutions were solvent evaporated on nitrocellulose paper.

FS28 Cleavage Assays in Solution: The substrate (FS28) cleavage assay was optimized in half-well microwell plates to minimize reagent consumption. The solution assay was performed using a similar protocol as the optimized conditions used during initial EC1 selection.⁸ The FS28 concentration was chosen to remain constant at 50 nM in all assays, based on previously reported EC1 monomer optimization.²¹ The low FS28 concentration was chosen to minimize substrate consumption and background from unhybridized FS28, while still allowing sufficient changes in fluorescence over time during the assay. The optimum FS28:EC1 DNAzyme concentration ratio was determined to be 1:50 (50 nM:

2.5 μM) by Aguirre *et al.*, in regards to the optimization of the monomer activity.²¹ The *E. coli* CIM was prepared by sonication without additional heating due to the success shown in previous assays using the EC1 monomer.¹⁷

The fluorescence enhancement of three constructs with different FS28:DNAzyme molar ratios were investigated to optimize the reaction in solution (Figure 3.3). The monomer, 2D RCA product, and 3D nanoflower constructs were investigated at concentrations of 1.0 μM , 1.5 μM , and 2.0 μM , with a constant concentration of 50 nM FS28. The optimized monomer concentration of 2.5 μM from previous reports was not used due to solubility limitations with the amplified DNA constructs, as the DNA precipitated from solution when the stock concentration was too high. The mutated EC1 sequence (EC1M), which is unable to cleave FS28, was also investigated and was used to establish the background signal from auto-cleavage, thus the fluorescence from wells containing EC1M was subtracted from that of each construct at each measured time point.

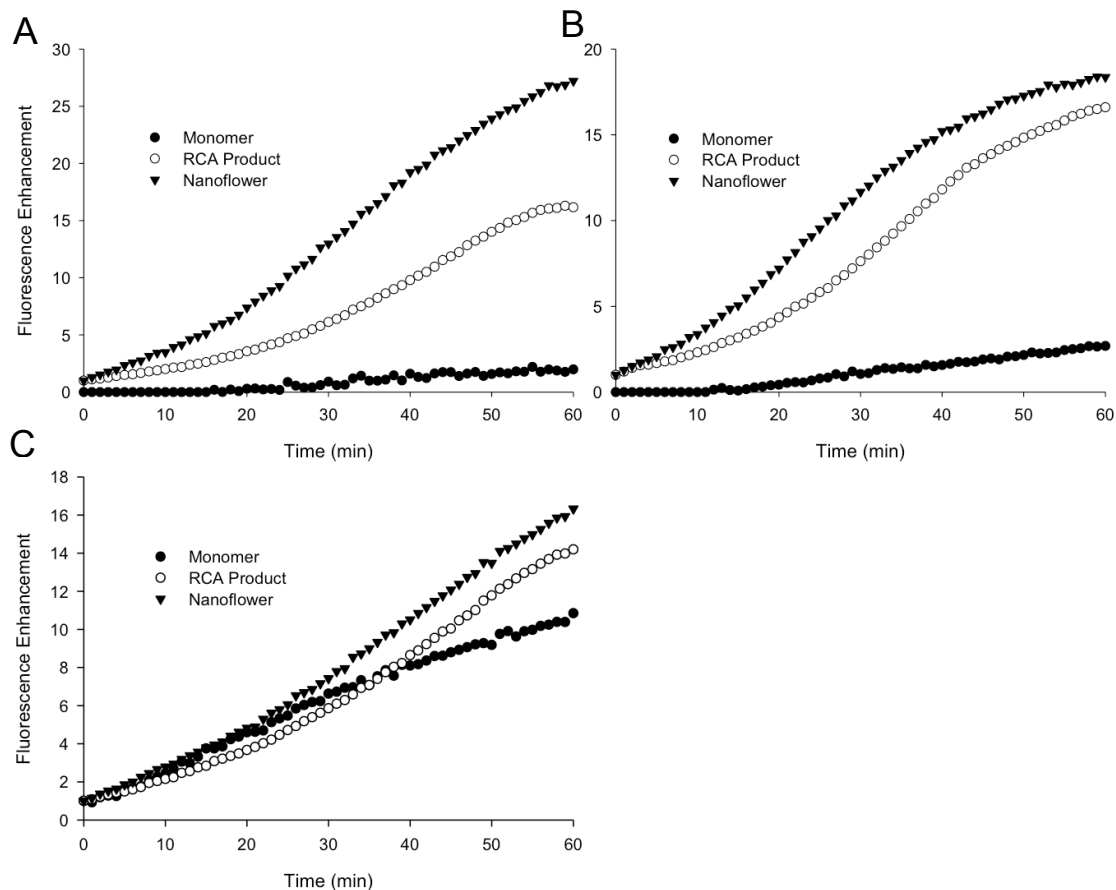


Figure 3.3. Optimization of the FS28 cleavage reaction using (A) 1.0 μM , (B) 1.5 μM , and (C) 2.0 μM of the various DNAzyme constructs. The background fluorescence produced in wells containing EC1M was subtracted from each construct over time. Initial fluorescence (F_0) corresponded to the fluorescence intensity immediately after adding 25 % (v/v) of the CIM (without heating). The nanoflower construct consistently exhibited greater fluorescence enhancement (F/F_0) than the monomer and 2D DNAzyme constructs.

The addition of CIM produced an increase in fluorescence for all DNAzyme constructs. It should be noted that the nanoflower and RCA product concentration was approximate since the actual size of each DNA oligomer was unknown and the concentration was calculated based on one repeat unit. The 3D nanoflowers exhibited the greatest fluorescence enhancement when the concentration was 1.0 μM . Meanwhile, the

monomer produced greater increases in fluorescence as the FS28:monomer concentration ratio decreased. Lower DNA construct concentrations were not investigated since the fluorescence enhancement using 1.0 μM of 3D nanoflowers seemed sufficient for future experiments. All future experiments used 1.0 μM of DNAzyme (1:20 FS28:DNAzyme).

An important point to note from the fluorescence assays was that the degree of fluorescence enhancement was generally much greater for concatenated DNAzymes relative to the monomeric form (up to 10-fold greater for 1.0 μM DNAzyme). This result may be related to a higher degree of hybridization of FS28 by the concatenated DNA relative to the monomer, or enhanced catalytic efficiency of the concatenated DNAzyme itself. The opposite trend in signalling levels with DNAzyme:FS28 ratio between the monomer and concatenated DNAzymes is not clear at this time, and will be the focus of future studies.

The selectivity of the DNA constructs for *E. coli* CIM was also investigated in solution, using 1.0 μM DNAzyme concentrations with 50 nM FS28 (1:20 ratio). The nanoflowers exhibited significant fluorescence enhancement in the presence of *E. coli* CIM in comparison to *Bacillus subtilis* CIM (Figure 3.4). *B. subtilis* was selected for comparison because the bacteria was used in counter selection during the initial development of the EC1 DNAzyme.⁸ It should be noted that the fluorescence produced by EC1M construct was used for background subtraction. In addition, the actual values of the fluorescent enhancements vary between days due to variation in the background fluorescence of EC1M and CIM.

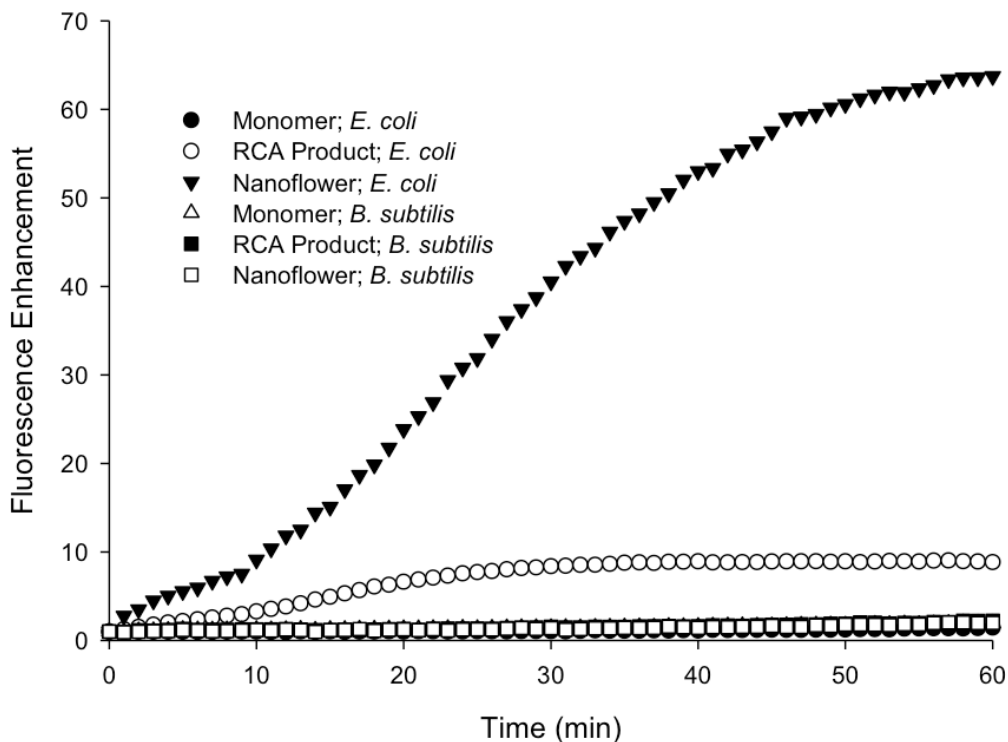


Figure 3.4. The fluorescence enhancement produced by the cleavage of FS28 (50 nM) by the three different DNAzyme types (1 μ M) in the presence of *E. coli* CIM or *B. subtilis* CIM. The background fluorescence produced by EC1M was subtracted from each measured value. The initial fluorescence corresponded to the fluorescence intensity measured immediately after adding the CIM to the wells.

In agreement with the data shown in Figure 3.3A, the 3D nanoflowers produced the largest signal enhancement in the presence of *E. coli* CIM, the 2D RCA products showed the next highest increase in fluorescence in the presence of *E. coli* CIM, whereas the monomer produced only a small signal enhancement. All of the DNAzyme constructs consistently showed no increase in fluorescent signal when *B. subtilis* was used however, thus confirming previously reported results regarding the selectivity of the EC1 monomer.^{8,21} Other *E. coli* strains were not investigated since previous reports showed that the strain did not change the signal response of the DNAzyme.²¹ These results indicate that the DNA concatemers cleaved FS28 specifically in the presence of *E. coli*,

which could allow the 2D RCA products and 3D nanoflower DNAzymes for use in *E. coli* detection using the 1: 20 DNAzyme: substrate ratio.

3.5 Conclusions

In conclusion, the nanoflowers were successfully folded into the proper structure and the initial nanoflower studies using *E. coli* CIM show that the fluorogenic substrate (FS28) was cleaved. All three of the EC1 DNAzyme constructs responded to *E. coli* CIM specifically, as shown by the lack of fluorescence when *B. subtilis* CIM was investigated.

In future work, the nanoflowers can be entrapped within sol-gel-derived silica materials for entrapment within columns. The columns could potentially be used to extract the unknown target in the *E. coli* CIM for identification using mass spectrometry. The substrate may need to be elongated to remain hybridized to the nanoflowers while flowing buffer and CIM through the columns. This adjustment may not be necessary if leaching is not a problem, however. In addition, reaction time should be minimized to avoid background nuclease activity and cleavage of the substrate, which can occur more as the CIM incubation time with the nanflowes is increased.

3.6 References

- (1) Liu, J.; Cao, Z.; Lu, Y. *Chem. Rev.* **2009**, *109*, 1948–1998.
- (2) Hui, C. Y.; Li, Y.; Brennan, J. D. *Chem. Mater.* **2014**, *26*, 1896–1904.
- (3) Rupcich, N.; Nutiu, R.; Li, Y.; Brennan, J. D. *Anal. Chem.* **2005**, *77*, 4771–4778.
- (4) Carrasquilla, C.; Brennan, J. D. *Methods* **2013**, *63*, 255–265.
- (5) Nutiu, R.; Li, Y. *J. Am. Chem. Soc.* **2003**, *125*, 4771–4778.
- (6) Carrasquilla, C.; Little, J. R. L.; Li, Y.; Brennan, J. D. *Chem. Eur. J.* **2015**, *21*, 7369–7373.
- (7) Shen, Z.; Wu, Z.; Chang, D.; Zhang, W.; Tram, K.; Lee, C.; Kim, P.; Salena, B. J.; Li, Y. *Angew. Chemie - Int. Ed.* **2016**, *55*, 2431–2434.
- (8) Ali, M. M.; Aguirre, S. D.; Lazim, H.; Li, Y. *Angew. Chemie - Int. Ed.* **2011**, *50*, 3751–3754.
- (9) Iliuk, A. B.; Hu, L.; Tao, W. A. *Anal. Chem.* **2011**, *83* (12), 4440–4452.
- (10) Liu, M.; Hui, C. Y.; Zhang, Q.; Gu, J.; Kannan, B.; Jahanshahi-Anbuhi, S.; Filipe, C. D. M.; Brennan, J. D.; Li, Y. *Angew. Chemie - Int. Ed.* **2016**, *55*, 2709–2713.
- (11) Cheglakov, Z.; Weizmann, Y.; Basnar, B.; Willner, I. *Org. Biomol. Chem.* **2007**, *5*, 223–225.
- (12) Liu, M.; Zhang, Q.; Chang, D.; Gu, J.; Brennan, J. D.; Li, Y. *Angew. Chemie* **2017**, *56*, 6142–6146.
- (13) Carrasquilla, C.; Kapteyn, E.; Li, Y.; Brennan, J. D. *Angew. Chem., Int. Ed.* **2017**, *56*, 10686–10690.
- (14) Zhao, W.; Ali, M. M.; Brook, M. A.; Li, Y. *Angew. Chemie - Int. Ed.* **2008**, *47*,

6330–6337.

- (15) Wang, F.; Lu, C. H.; Willner, I. *Chem. Rev.* **2014**, *114*, 2881–2941.
- (16) Wang, F.; Lu, C. H.; Liu, X.; Freage, L.; Willner, I. *Anal. Chem.* **2014**, *86*, 1614–1621.
- (17) Liu, M.; Zhang, Q.; Li, Z.; Gu, J.; Brennan, J. D.; Li, Y. *Nat Commun* **2016**, *7*, 12074–12080.
- (18) Guo, Y.; Wang, Y.; Liu, S.; Yu, J.; Wang, H.; Wang, Y.; Huang, J. *Biosens. Bioelectron.* **2016**, *75*, 315–319.
- (19) Zhang, W.; Feng, Q.; Chang, D.; Tram, K.; Li, Y. *Methods* **2016**, *106*, 66–75.
- (20) Tram, K.; Kanda, P.; Li, Y. *J. Nucleic Acids* **2012**, *2012*, 1–8.
- (21) Aguirre, S. D.; Ali, M. M.; Salena, B. J.; Li, Y. *Biomolecules* **2013**, *3*, 563–577.
- (22) Nutiu, R.; Li, Y. *Methods* **2005**, *37*, 16–25.
- (23) Zhu, G.; Hu, R.; Zhao, Z.; Chen, Z.; Zhang, X.; Tan, W. *J. Am. Chem.* **2013**, *135*, 1–10.
- (24) Lv, Y.; Hu, R.; Zhu, G.; Zhang, X.; Mei, L.; Liu, Q.; Qiu, L.; Wu, C.; Tan, W. *Nat. Protoc.* **2015**, *10*, 1508–1524.

3.7 Appendix

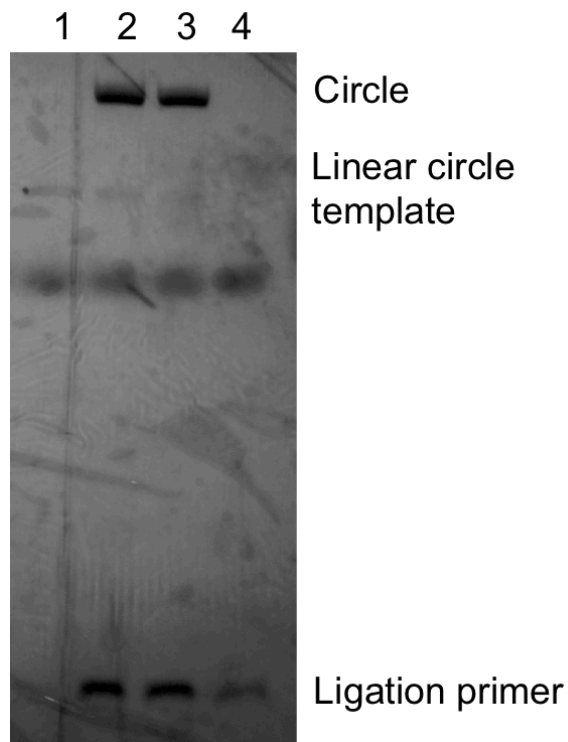


Figure S3.1. Circle ligation was successful (lanes 2 and 3), as indicated in the 10 % dPAGE gel used for purification. Despite the circle having the same molecular weight as the linear circle (lane 1, band above smeared dye), the circle cannot move through the gel as easily which results in a shifted band. The primer is present near the bottom of the gel.

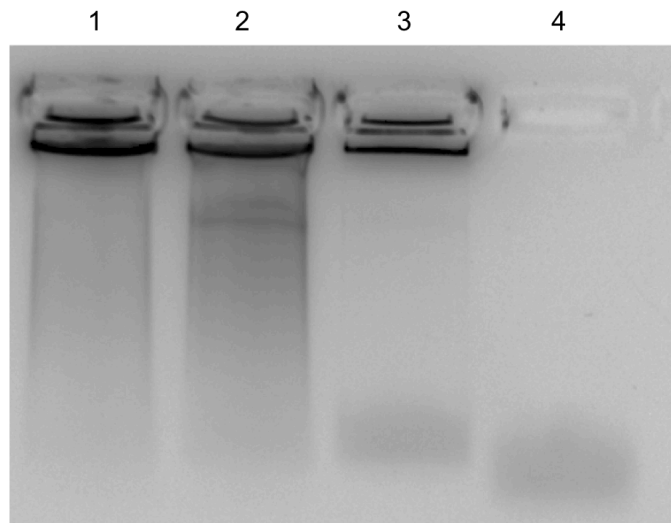


Figure S3.2. RCA of the purified circle resulted in thick bands with smearing on the 0.6 % agarose gel, which indicates concatemers present in the sample (lanes 1 and 2). Lane 3 shows the results of the negative control, meanwhile lane 4 contains only circle.

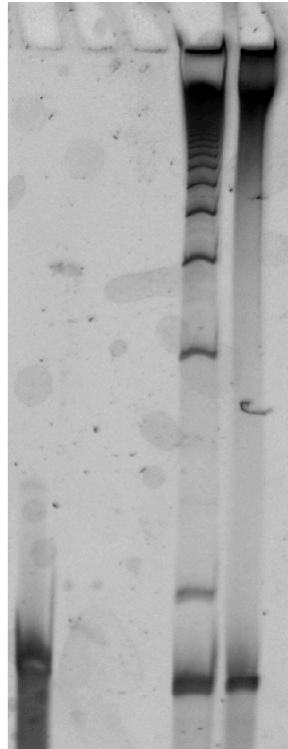


Figure S3.3. Restriction enzyme digestion produced DNA strands of various lengths based on the extent of digestion that occurred on the various sized concatemers. The negative control did not contain restriction enzyme, which accounts for the thick smear. The bottom band corresponds to the size of the monomer.

Table S3.1. Sequences of the DNA oligonucleotides used in this work.

Name of DNA Oligonucleotide	Sequence (5' → 3')
Circular template: anti-EC1 (85 bp)	AACTATAAGA GCATCCACAC AACTGTAAAG AAATCCATCC CCACACAGTG TAGTGTTCCG GTCGCAGGTC TCGACAACGC ACATC
EC1 template primer (21 bp)	TGCTCTTATA GTTGATGTGC G
EC1 monomer (71 bp)	GATGTGCGTT GTCGAGACCT GCGACCGGAA CACTACACTG TGTGGGGATG GATTTCTTTA CAGTTGTGTG (inverted T)
Mutated version of monomer: EC1M (70 bp)	GATGTGCGTT GAGCTCACCT GCGACCGGAA CACTACTGAC ACTGGGGATG GATTTCTTTA CAGTTGTGTG
Chimeric DNA/RNA substrate: FS28 (28 bp) F = fluorescein-dT R = riboadenosine Q = dabcyI-dT	ACTCTTCCTA GCFRQGGTTC GATCAAGA
Complementary sequence for HpaII digestion: compH (18 bp)	AGTGTTCGG TCGCAGGT

CHAPTER 4 | CONCLUSIONS

4.1 Summary and Future Outlook

The results from this work support the hypothesis that protein detection is possible using aptamer entrapment along sol-gel-derived biohybrid columns. The initial high-throughput material screen determined the ideal macroporous material that prevented concatemeric aptamer leaching while maintaining structure-switching capabilities for fluorescence detection along monolithic capillary columns. The concatemers responded in a concentration-dependent manner for the detection of small molecules and proteins. Sol-gel-derived material entrapment was able to be performed with the aptamers due to the previous work performed that demonstrated the effectiveness of concatemeric aptamers,¹ unlike the EC1 DNAzyme which had not been concatenated using RCA previously.

Following the success in using aptamers for biosensing, the FNA was changed to the EC1 DNAzyme. The concatenation and folding of the EC1 nanoflowers was successfully accomplished, and the nanoflower DNAzymes were shown to cleave the FS28 substrate in the presence of *E. coli* CIM. The nanoflowers cleaved the fluorogenic substrate with better efficacy than the monomer DNAzyme. The initial promising results involving an increase in fluorescence over time with the nanoflowers and substrate when in the presence of *E. coli* CIM may allow the EC1 nanoflowers for entrapment within materials. Additionally, it should be noted that this seems to be the first instance that DNAzymes were used in nanoflower form rather than as a simple concatenated product.

Concatenated DNAzyme activity in solution was investigated for the eventual goal of entrapping the DNAzyme-based nanoflowers in sol-gel-derived materials. Once active

nanoflowers are created, the material screen would need to be repeated because aptamers and DNAzymes do not use the same mechanism of action to produce a fluorescent signal.² Eventually, the nanoflowers may be able to be entrapped within sol-gel-derived capillary columns for target detection and extraction. The unknown EC1 DNAzyme target may be able to be identified using mass spectrometry following column extraction.³

Using capillary columns for affinity chromatography offers the unique advantage that compounds or biomolecules can be extracted and purified from a mixture. There was still a significant amount of optimization using the DNAzyme nanoflowers required prior to column extraction, however monolithic columns of these types have been used before for small molecule extraction.³ With the advent of macroporous monolithic columns that can detect large biomolecules, it is feasible to hypothesize that these FNA-based columns can be modified for target extraction. Large biomolecules, such as proteins and viruses, could not be extracted using monolithic columns prior to this work. The fabrication of monolithic columns entrapping concatemeric FNAs have the potential for the efficient extraction and purification of large biomolecules using various protocols, such as bio-solid-phase extraction.

4.2 References

- (1) Carrasquilla, C.; Little, J. R. L.; Li, Y.; Brennan, J. D. *Chem. Eur. J.* **2015**, *21*, 7369–7373.
- (2) Carrasquilla, C.; Brennan, J. D. *Methods* **2013**, *63*, 255–265.
- (3) Forsberg, E. M.; Brennan, J. D. *Anal. Chem.* **2014**, *86*, 8457–8465.